Journal of Sound and Vibration (1998) **216**(5), 809–849
Article No. sv981704

L-, T-, AND CROSS-JOINTS OF LINED DUCTS

F. P. MECHEL
D-71120 *Grafenau* 1, *Germany*

(*Received* 13 *June* 1997, *and in final form* 16 *April* 1998)

Much effort has been spent to increase the attenuation of lined ducts at low frequencies with only a minor increase of the blocking of the duct by thick silencers, in order to keep the stationary flow resistance of the silencer at low values. There exists a similar problem at high frequenices, where the attenuation goes down at about the square of the inverse frequency as soon as the frequency limit of ray formation is exceeded at which the free duct is about half a wavelength wide. The principal remedy of the problem, to choose narrow ducts, would increase the aerodynamic resistance. The ray-acoustical background of the low attenuation at high frequencies suggests using the existing corners of the ductwork into which the silencer is inserted for the generation of high-frequency attenuation. A naïve idea is to assume that the exciting sound ray of the inlet duct should be absorbed by an absorber on the corner wall opposite this duct, thereby avoiding the excitation of the outlet branch of the duct. Such a corner absorber could be applied in wide ducts also. This paper presents theories of joints of acoustically lined ducts with separate sound absorbers at the corner walls. The numerical results will show that high transmission losses can indeed be achieved at high frequencies, but the mechanism of the corner attenuation is not so much the absorption by the corner absorber, but more the (cut-off) attenuation of higher modes in the lined outlet branch of the duct.

1. INTRODUCTION

High attenuation values of silencers in technical duct systems are in conflict with the requirement of a low aerodynamic flow resistance. High attenuation at low frequencies needs thick linings, high attenuation at high frequencies demands small distances between the linings. A first compromise in this conflict is the use of baffle type silencers. Many papers deal with the extension of the low frequency range of performance of silencers with only a minor increase in the absorber thickness, e.g., with specially designed resonator absorbers. The mirror reflected problem at high frequencies has attracted less interest. Cremer [1] in 1953 pointed out the principal limitation of attenuation towards higher frequencies by the limit of ray formation, where the free duct width is about half a wavelength. The interaction between the lining and the sound wave (the least attenuated mode) becomes weak above that frequency; the consequence is a slope of the attenuation with about $1/f^2$ (f = frequency). It is generally accepted, therefore, that a high frequency end of the performance range of a silencer is combined with narrow ducts. This too increases the aerodynamic resistance of the silencer.

0022–460X/98/400809 + 41 $30.00/0

On the other hand, the ray-acoustical explanation of the high frequency slope of the attenuation suggests a solution of the problem. One assumes that there are duct corners in most duct systems which contain the silencer. If a sound absorber is placed at the duct wall opposite the duct branch with the incident sound wave, then the sound could be effectively absorbed, just because of the ray formation of the sound wave: i.e., with high absorption coefficients at high frequencies. Presumably, the excitation of the outlet branch of the duct would be reduced. This suggestion evidently takes away the high frequency sound reduction from the silencer and places it into the duct corners.

Brittain *et al*. [2] reported about measurements of the transmission loss of joints of lined ducts with different angles. Later papers about joints of ducts mainly deal with rigid ducts, such as those of Lippert [3, 4], Hubert and Said [5], Redmore and Mulholland [6], Bruggeman [7], and Cummings [8] treated a related problem with his theoretical study of lined plenum chambers in ducts. The theory of section 3 below is similar to a method which Lapin [9] applied to ducts with side branches. However, he considered only rigid ducts and branches and restricted his analysis to the fundamental mode only in the side branch. A later paper by Lapin [10], dealt with lined ducts, but there the analysis was reduced to a technique of equivalent circuits. Corners and junctions of (lined) ducts often are objects for numerical methods, such as FEM or BEM.

Two theoretical methods will be described below. The first method (in sections 2 and 3) is similar to the method applied by Lapin in that it assumes a fictitious volume source in the end plane of one of the joining ducts which describes the scattering of that duct into the corner region and the other duct. The task will be to determine the amplitude of the fictitious source. Depending on where the additional absorber of the corner is placed, the fictitious source is placed in the end plane of either the entrance duct or of the exit duct. This method of fictitious sources is described below, although it is an approximate method only, because it is a continuation of the theoretical line in Lapin's papers, and because the computing time in numerical applications is low. The second method (in section 4) is an exact theory from its outline. It introduces two fictitious duct sections for the corner region, which are lined with the extra absorbers in the corner, and then proceeds essentially with standard modal analysis methods.

We start with the theoretical treatment of L-joints of lined ducts. It will be shown in section 5 how the theory can be applied to T- and cross-joints. The objects of the two following sections are depicted in Figure 1. Two ducts $i = 1, 2$ which form the zones I and II join in the zone III of the corner region. The ducts have widths $2h_i$ and are lined with locally reacting absorbers having surface admittances G_i. The incident sound wave p_i comes from the branch $i = 1$; it is assumed to be the mode with mode index μ of the inlet duct. In the arrangement of Figure 1(a), the corner wall opposite the exit duct is lined with a distinct locally reacting absorber with a surface admittance G_3. In Figure 1(b) this absorber is placed at the wall opposite the entrance duct. The system of co-ordinates x, y is placed along the centres of the ducts. First, constant fields are assumed in the z-direction; it will be shown in section 5 how the theory and its results have to be modified for ducts with finite dimension in the z-direction. Although the

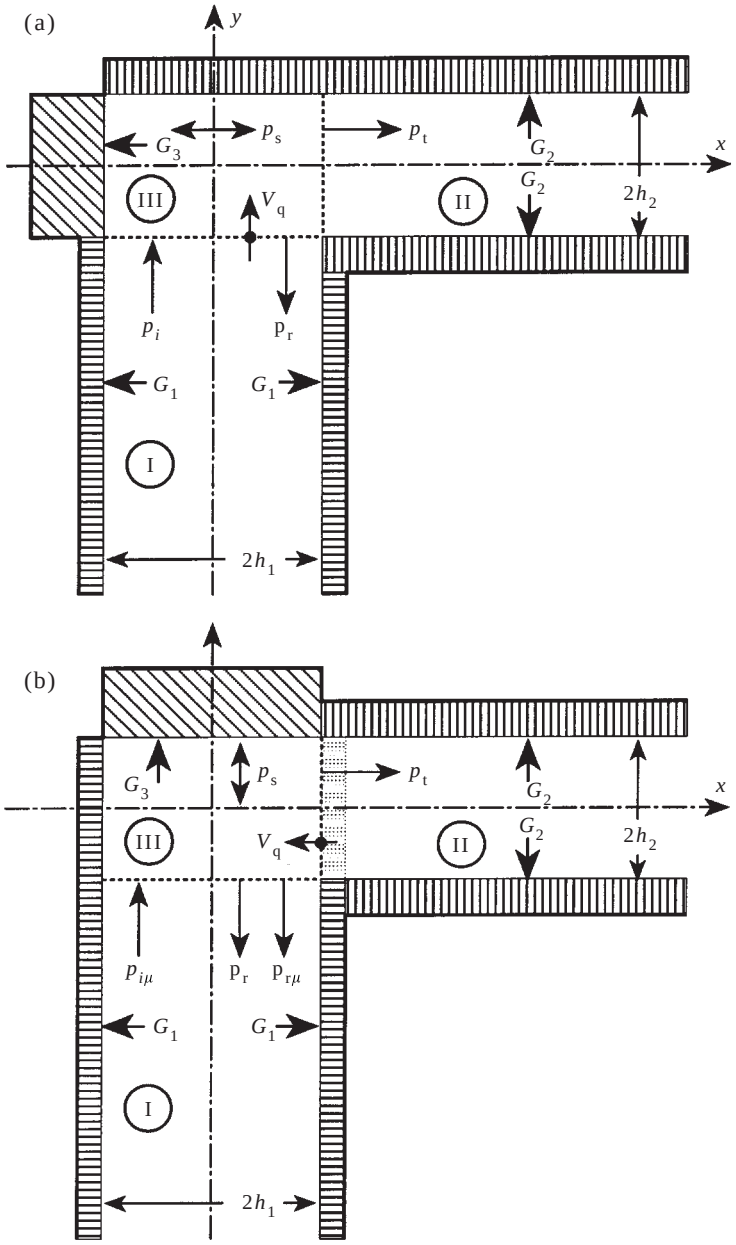

Figure 1. L-joints of lined ducts with absorbers in the corner area. The arrangement (a) is the object of section 2; the arrangement (b) is the object of section 3.

arrangement of Figure 1(b) corresponds better to the suggestion outlined above, we begin with the arrangement of Figure 1(a); here the theory of the two following sections is easier to describe. This arrangement is needed for a generalization to T-joints in which the sound wave comes from the side branch.

The reason, why the absorbers here are supposed to be locally reacting is that the relation of orthogonality of modes in ducts with locally reacting linings is much

easier to handle than the relation of orthogonality of modes with bulk reacting linings. A lot of experience shows that local absorbers can be used as approximations to bulk absorbers, if the flow resistance of the latter is high enough.

The theory of the two following sections makes use of a fictitious particle velocity source with a distribution V_q in one of the duct ends. The sound field in the other duct will be developed as a function of V_q. When the lateral distribution of V_q is synthesized by modes of that duct, a linear, inhomogeneous system of equations for the mode amplitudes is derived from the boundary conditions at the end planes of the ducts towards zone III. The sound fields are known after the solution of that system of equations. The theory with the auxiliary source V_q is approximate from the outset, because only a velocity source is assumed; a complete theory would need an additional sound pressure source. The theory can be tested by assuming $h_1 = h_2$ and $G_1 = G_2 = G_3$ in both arrangements of Figure 1, because then the arrangements are identical to each other, but the derivations are quite different.

Because of the approximate character of the solutions as outlined above, and because of some restrictions of these theories in the special case of rigid duct walls (explained in section 5) a theory based on a modal analysis of the problem is derived in section 4. This theory is exact in the framework of a Fourier analysis: the boundary conditions at the end planes of the ducts are satisfied in the sense of a minimum least square error over the cross-section of these planes. The error can be reduced by a large number of duct modes in the numerical computations. Each of the theories described below has its own merits. The theory of section 2 has the lowest precision, but it is the fastest in numerical computations. The theory of section 3 has a better precision, but the computing time is about twice as long as in section 2. The theory of section 4 with the modal analysis has the best precision and the highest generality; its computing time is again increased by a factor of two. Both a critical inspection of the results of the theories with the auxiliary source V_q, and the comparison to results of the modal analysis show that the errors of the first theories are in the near fields of the transition planes. Only the far field in the exit duct is important in most technical applications, where the near fields have decayed and the least attenuated mode will prevail. The results are good under these conditions, so the methods of sections 2 and 3 can be applied for the computation of the transmission loss of the duct joint which is based on the level difference of the least attenuated mode in the exit duct (at the entrance plane of the duct) to the incident mode (at the exit plane of the entrance duct).

2. L-JOINT WITH ABSORBER OPPOSITE THE EXIT DUCT

Quantities in the two ducts $i = 1, 2$ are indicated by i appended to the quantity (with the exception of the incident wave p_i). The incident wave $p_i(x, y)$ generates a reflected wave $p_r(y, y)$ which in this section is assumed to be generated at the exit plane of the entrance duct. A transmitted wave $p_t(x, y)$ will be generated in zone II of the exit duct. The field $p_s(x, y)$ in the corner area of zone III is called

the "scattered field". The superposition $p_i + p_r$ will produce a velocity distribution $V_q(x_0, y_0)$ in the exit plane $y_0 = -h_2$, $x_0 = (-h_1, h_1)$ of the entrance duct. V_q is assumed to be the source of p_s and p_t. First, the fields p_s and p_t are formulated as functions of V_q. Then p_r is synthesized by modes of the entrance duct, with mode amplitudes A_m. These amplitudes are introduced into V_q by the boundary condition for the velocity $V_q(x_0, y_0) = v_{iy}(x_0 + y_0) + v_{ry}(x_0, y_0)$. Finally, the pressure boundary condition $p_i(x_0, y_0) + p_r(x_0, y_0) = p_s(x_0, y_0)$ will give the desired system of equations for the A_m. All sound fields will be known after the solution of that system of equations.

The sound fields in both ducts (with a time factor $e^{j\omega t}$) are composed by duct modes with the shapes

$$qi_k(\eta_i)\, e^{\pm \gamma i_k \xi_i}, \quad i = 1, 2, \quad k = 0, 1, 2, \ldots, \quad \eta_i = \begin{Bmatrix} x, & i = 1 \\ y, & i = 2 \end{Bmatrix}, \quad \xi_i = \begin{Bmatrix} y, & i = 1 \\ x, & i = 2 \end{Bmatrix}. \tag{1}$$

The mode profiles for modes which are symmetrical or antisymmetrical with respect to the duct centres respectively are

$$qi_k(\eta_i) = \begin{Bmatrix} \cos(\varepsilon i_k \eta_i), & k = 0, 2, 4, \ldots \\ \sin(\varepsilon i_k \eta_i), & k = 1, 3, 5, \ldots \end{Bmatrix}. \tag{2}$$

One is free to identify $qi_k(\eta_i) \equiv qi_k(\varepsilon i_k \eta_i)$ when the wave number εi_k is shown. Further use is made of the freedom in the enumeration of modes and even indices are attributed to symmetrical modes and odd numbers to antisymmetrical modes. The wave equation is satisfied if

$$\gamma i_k^2 = \varepsilon i_k^2 - k_0^2 \tag{3}$$

holds, and the boundary conditions at the surface of the duct lining lead to the characteristic equations

$$\varepsilon i_k h_i qi_k'(\varepsilon i_k h_i) = -jk_0 h_i Z_0 G_i qi_k(\varepsilon i_k h_i) = -jU_i qi_k(\varepsilon i_k h_i) \tag{4}$$

for $\varepsilon i_k h_i$. The prime indicates the derivative with respect to the shown argument. The "absorber function" $U_i = k_0 h_i Z_0 G_i$ has been introduced, which is the only quantity in the characteristic equations containing information about the absorber of the lining. k_0, Z_0 are the free-field wave number and the free-field wave impedance. The relations

$$\begin{gathered} qi_k(-h_i) = (-1)^k qi_k(h_i), \quad qi_k'(-h_i) = (-1)^{k+1} qi_k'(h_i), \\ qi_k'(h_i) = -j(U_i/h_i) qi_k(h_i), \quad qi_k'(-h_i) = j(-1)^k (U_i/h_i) qi_k(h_i), \\ qi_k''(\eta_i) = -\varepsilon i_k^2 qi_k(\eta_i). \end{gathered} \tag{5}$$

are applied several times. The first two of equations (5) contain the symmetry relations of even and odd modes, the second two contain their characteristic equations, and the last contains the second derivatives.

The modes in the duct i are orthogonal to each other over the duct width with the norms

$$Ni_k := \frac{1}{2h_i}\int_{-h_i}^{h_i} qi_k^2(\eta_i)\,\mathrm{d}\eta_i = \frac{1}{2}\left[1 + (-1)^k \frac{\sin(2\varepsilon i_k h_i)}{2\varepsilon i_k h_i}\right]. \tag{6}$$

With the assumed velocity source $V_q(x_0, y_0)$ in the exit plane $y_0 = -h_2$, $x_0 = (-h_1, h_1)$ of the entrance duct, the inhomogeneous wave equation for the contribution $\mathrm{d}p_2$ of a source element $\mathrm{d}x_0$

$$(\Delta + k_0^2)\,\mathrm{d}p_2(x, y) = -\mathrm{j}k_0 Z_0 V_q(x_0, y_0)\,\mathrm{d}x_0\,\delta(x - x_0)\,\delta(y - y_0) \tag{7}$$

holds in the exit duct which now also includes zone III. If one develops $\delta(y - y_0)$ by

$$\delta(y - y_0) = \sum_n a_n q_n^2(y), \tag{8}$$

the application of

$$\frac{1}{2h_2}\int_{-h_2}^{h_2} \ldots q2_n(y)\,\mathrm{d}y \tag{9}$$

immediately gives

$$a_n = q2_n(y_0)/2h_2 N2_n. \tag{10}$$

The contribution of the volume source element $V_q(x_0, y_0)\,\mathrm{d}x_0$ of the exit duct is developed in duct modes

$$\mathrm{d}p_2(x, y) = \sum_n F_n(x) q2_n(y). \tag{11}$$

This, inserted into the wave equation (7), gives

$$\left(\frac{\mathrm{d}^2}{\mathrm{d}x^2} - \gamma 2_n^2\right)F_n(x) = -\mathrm{j}k_0 Z_0 V_q(x_0, y_0)\,\mathrm{d}x_0 \frac{q2_n(y_0)}{2h_2 N2_n}\,\delta(x - x_0). \tag{12}$$

It is known that the Green function $g(x|x_0)$ of a unit source, with the inhomogeneous wave equation

$$\left(\frac{\mathrm{d}^2}{\mathrm{d}x^2} - \gamma 2_n^2\right)g(x|x_0) = -\delta(x - x_0), \tag{13}$$

is determined such that it satisfies the homogeneous wave equation and the boundary conditions so that $g(x|x_0)$ is continuous at x_0, but the derivatives from both sides have a unit difference:

$$g(x_{0+}|x_0) = g(x_{0-}|x_0), \qquad \frac{\mathrm{d}}{\mathrm{d}x}g(x|x_0)|_{x_{0+}} - \frac{\mathrm{d}}{\mathrm{d}x}g(x|x_0)|_{x_{0-}} = -1. \tag{14}$$

If the exit duct were infinitely long in both directions, the Green function

$$g(x|x_0) = \frac{1}{2\gamma 2_n}\,\mathrm{e}^{-g2_n|x-x_0|} = \begin{cases} \dfrac{1}{2\gamma 2_n}\,\mathrm{e}^{-\gamma 2_n(x-x_0)}, & x > x_0 \\ \dfrac{1}{2\gamma 2_n}\,\mathrm{e}^{+\gamma 2_n(x-x_0)}, & x < x_0 \end{cases}, \tag{15}$$

would evidently satisfy all requirements. In the duct with the termination in G_3 at $x = -h_1$, there will be modes in the Green function running towards this termination. They will be reflected there with the modal reflection factors:

$$r_n = (\mathrm{j}\gamma 2_n/k_0 + Z_0 G_3)/(\mathrm{j}\gamma 2_n/k_0 - Z_0 G_3). \tag{16}$$

If these reflections are added to expression (15), taking into account the propagation from the source point x_0 to the point of reflection at $-h_1$ and back to the field point x, one gets the Green function for our problem:

$$g(x|x_0) = \left\{ \begin{array}{ll} \dfrac{1}{2\gamma 2_n}\,\mathrm{e}^{-\gamma 2_n(x-x_0)} + r_n\,\mathrm{e}^{-\gamma 2_n(x+x_0+2h_1)}, & x > x_0 \\ \dfrac{1}{2\gamma 2_n}\,\mathrm{e}^{+\gamma 2_n(x-x_0)} + r_n\,\mathrm{e}^{-\gamma 2_n(x+x_0+2h_1)}, & x < x_0 \end{array} \right\}. \tag{17}$$

It can be easily checked that equation (14) is valid for this expression. So the contribution of $V_q(x_0, y_0)\,\mathrm{d}x_0$ to the sound field in the exit duct is

$$\mathrm{d}p_2(x, y) = \mathrm{j}\,\frac{k_0 Z_0}{4}\,V_q(x_0, y_0)\,\mathrm{d}x_0 \sum_n \frac{q2_n(y_0)q2_n(y)}{\gamma 2_n h_2 N2_n}$$

$$\times\,[\mathrm{e}^{\mp\gamma 2_n(x-x_0)} + \mathrm{r_n}\,\mathrm{e}^{-\gamma 2_n(x+x_0+2h_1)}], \qquad \left\{ \begin{array}{l} x > x_0 \\ x < x_0 \end{array} \right\}. \tag{18}$$

By integration of the elementary contributions the transmitted field p_t in the exit duct becomes

$$p_t(x, y) = \mathrm{j}\,\frac{k_0 Z_0}{4} \sum_n \frac{q2_n(y_0)q2_n(y)}{\gamma 2_n h_2 N2_n}\,\mathrm{e}^{-\gamma 2_n x}$$

$$\times \left[\int_{-h_1}^{h_1} \mathrm{e}^{+\gamma 2_n x_0} V_q(x_0, y_0)\,\mathrm{d}x_0 + r_n\,\mathrm{e}^{-2\gamma 2_n h_1} \int_{-h_1}^{h_1} \right.$$

$$\left. \times\,\mathrm{e}^{-\gamma 2_n x_0} V_q(x_0, y_0)\,\mathrm{d}x_0 \right], \tag{19}$$

and the scattered field in zone III is

$$p_s(x, y) = \mathrm{j}\frac{k_0 Z_0}{4}\sum_n \frac{q2_n(y_0)q2_n(y)}{\gamma 2_n h_2 N2_n}$$

$$\times\left[\mathrm{e}^{-\gamma 2_n x}\left(\int_{-h_1}^{x}\mathrm{e}^{+\gamma 2_n x_0}V_q(x_0, y_0)\,\mathrm{d}x_0 + r_n\,\mathrm{e}^{-2\gamma 2_n h_1}\int_{-h_1}^{h_1}\right.\right.$$

$$\left.\left.\times\,\mathrm{e}^{-\gamma 2_n x_0}V_q(x_0, y_0)\,\mathrm{d}x_0\right)\right.$$

$$\left.+\,\mathrm{e}^{+\gamma 2_n x}\int_{x}^{h_1}\mathrm{e}^{-\gamma 2_n x_0}V_q(x_0, y_0)\,\mathrm{d}x_0\right]. \tag{20}$$

For conciseness of the equations, the notation $V_q(x_0, y_0)\to V_q(x_0)$ with $y_0 = -h_2$ and the integrals

$$IA_n(x) = \frac{\mathrm{j}}{2h_1}\int_{-h_1}^{x}\mathrm{e}^{+\gamma 2_n x_0}V_q(x_0)\,\mathrm{d}x_0, \qquad IB_n(x) = \frac{\mathrm{j}}{2h_1}\int_{x}^{h_1}\mathrm{e}^{-\gamma 2_n x_0}V_q(x_0)\,\mathrm{d}x_0. \tag{21, 22}$$

are introduced. Then one gets

$$p_t(x, y) = \frac{k_0 Z_0}{2}\frac{h_1}{h_2}\sum_n \frac{q2_n(y_0)q2_n(y)}{\gamma 2_n N2_n}\,\mathrm{e}^{-\gamma 2_n x}[IA_n(h_1) + r_n\,\mathrm{e}^{-2\gamma 2_n h_1}IB_n(-h_1)], \tag{23}$$

$$p_s(x, y) = \frac{k_0 Z_0}{2}\frac{h_1}{h_2}\sum_n \frac{q2_n(y_0)q2_n(y)}{\gamma 2_n N2_n}$$

$$\times\,[\mathrm{e}^{-\gamma 2_n x}(IA_n(x) + r_n\,\mathrm{e}^{-2\gamma 2_n h_1}IB_n(-h_1) + \mathrm{e}^{+\gamma 2_n x}IB_n(x)]. \tag{24}$$

With the reflected field p_r written as a mode sum, the field in the entrance duct is

$$p_I(x, y) = p_i(x, y) + p_r(x, y) = P_i q1_\mu(x)\,\mathrm{e}^{-\gamma 1_\mu y} + \sum_m A_m q1_m(x)\,\mathrm{e}^{+\gamma 1_m y}. \tag{25}$$

One evidently has $V_q(x_0) = v_{Iy}(x, -h_2)$ and therefore

$$V_q(x_0) = \frac{\mathrm{j}}{k_0 Z_0}\sum_m [A_m\gamma 1_m\,\mathrm{e}^{-\gamma 1_m h_2} - \delta_{m,\mu}P_i\gamma 1_\mu\,\mathrm{e}^{+\gamma 1_\mu h_2}]q1_m(x_0)$$

$$= \frac{\mathrm{j}}{k_0 Z_0}\sum_m \gamma 1_m C_{m-}\,q1_m(x_0), \tag{26}$$

where the abbreviation

$$C_{m\pm} = A_m \, \mathrm{e}^{-\gamma 1_m h_2} \pm \delta_{m,\mu} P_i \, \mathrm{e}^{+\gamma 1_\mu h_2} \tag{27}$$

has been introduced and the Kronecker symbol $\delta_{m,\mu}$. Recall that the boundary condition for the particle velocity at the end plane of the entrance duct is satisfied by the above formulation of the auxiliary source V_q. The boundary conditions at the entrance plane of the exit duct are also satisfied, because $p_s = p_t$ in that plane and also $\partial p_s/\partial x = \partial p_t/\partial x$, as can be easily seen from equations (23) and (24). The remaining boundary condition for the sound pressure $p_s(x, -h_2) \overset{!}{=} p_I(x, -h_2)$ now reads (the sign $\overset{!}{=}$ indicates that it is a requirement introduced by the boundary condition; it is continuous in x, and it shall be transformed into a system of equations for the unknown amplitudes):

$$\begin{aligned}\sum_m C_{m+} q1_m(x) \overset{!}{=} \frac{\mathrm{j}}{2}\frac{h_1}{h_2}\sum_m \gamma 1_m C_{m-} \\ \times \sum_n \frac{q2_n^2(h_2)}{\gamma 2_n N2_n}\left[\mathrm{e}^{-\gamma 2_n x}(IA_{m,n}(x) + r_n \, \mathrm{e}^{-2\gamma 2_n h_1} IB_{m,n}(-h_1))\right. \\ \left. + \mathrm{e}^{+\gamma 2_n x} IB_{m,n}(x)\right],\end{aligned} \tag{28}$$

wherein the following integrals appear,

$$IA_{m,n}(x) = Ia_{m,n}(x) - Ia_{m,n}(-h_1), \quad IB_{m,n}(x) = Ib_{m,n}(h_1) - Ib_{m,n}(x), \tag{29a}$$

with

$$\begin{aligned}Ia_{m,n}(x) &= \frac{1}{2h_1}\int^x \mathrm{e}^{+\gamma 2_n y} q1_m(y)\,\mathrm{d}y = \frac{\mathrm{e}^{\gamma 2_n x}}{2h_1(\gamma 2_n^2 + \epsilon 1_m^2)}\left[\gamma 2_n q1_m(x) - q1'_m(x)\right], \\ Ib_{m,n}(x) &= \frac{1}{2h_1}\int^x \mathrm{e}^{-\gamma 2_n y} q1_m(y)\,\mathrm{d}y = \frac{-\mathrm{e}^{-\gamma 2_n x}}{2h_1(\gamma 2_n^2 + \epsilon 1_m^2)}\left[\gamma 2_n q1_m(x) + q1'_m(x)\right].\end{aligned} \tag{29b}$$

The orthogonality integral operator

$$\frac{1}{2h_1}\int_{-h_1}^{h_1} \ldots q1_k(y)\,\mathrm{d}y, \tag{30}$$

is applied to both sides of equation (28). The left-side will give $C_{k+} N1_k$. The first and third term in the brackets of the right-side will give

$$\begin{aligned}\frac{1}{2h_1}\int_{-h_1}^{h_1} \mathrm{e}^{-\gamma 2_n x} IA_{m,n}(x) q1_k(x)\,\mathrm{d}x + \frac{1}{2h_1}\int_{-h_1}^{h_1} \mathrm{e}^{+\gamma 2_n x} IB_{m,n}(x) q1_k(x)\,\mathrm{d}x \\ = \frac{2\delta_{m,k}\gamma 2_n N1_k}{2h_1(\gamma 2_n^2 + \epsilon 1_m^2)}\end{aligned}$$

$$- Ib_{m,n}(h_1)\frac{1}{2h_1}\int_{-h_1}^{h_1} \mathrm{e}^{+\gamma 2_n x} q1_k(x)\,\mathrm{d}x - Ia_{m,n}(-h_1)\frac{1}{2h_1}\int_{-h_1}^{h_1} \mathrm{e}^{-\gamma 2_n x} q1_k(x)\,\mathrm{d}x$$

$$= \frac{2\delta_{m,k}\gamma 2_n N1_k}{2h_1(\gamma 2_n^2 + \varepsilon 1_m^2)}$$

$$- Ib_{m,n}(h_1)(Ia_{k,n}(h_1) - Ia_{k,n}(-h_1)) - Ia_{m,n}(-h_1)(Ib_{k,n}(h_1) - Ib_{k,n}(-h_1)), \quad (31)$$

with

$$Ib_{m,n}(h_1)(Ia_{k,n}(h_1) - Ia_{k,n}(-h_1))$$

$$= \frac{-q1_m(h_1)q1_k(h)}{4h_1^4(\gamma 2_n^2 + \varepsilon 1_m^2)(\gamma 2_n^2 + \varepsilon 1_k^2)}[\gamma 2_n h_1 - \mathrm{j}U_1]$$

$$\times [\gamma 2_n h_1(1 - (-1)^k \mathrm{e}^{-2\gamma 2_n h_1}) + \mathrm{j}U_1(1 + (-1)^k \mathrm{e}^{-2\gamma 2_n h_1})], \quad (32a)$$

$$Ia_{m,n}(-h_1)(Ib_{k,n}(h_1) - Ib_{k,n}(-h_1))$$

$$= \frac{(-1)^m q1_m(h_1)q1_k(h_1)}{4h_1^4(\gamma 2_n^2 + \varepsilon 1_m^2)(\gamma 2_n^2 + \varepsilon 1_k^2)}[\gamma 2_n h_1 - \mathrm{j}U_1]$$

$$\times [\gamma 2_n h_1((-1)^k - \mathrm{e}^{-2\gamma 1_n h_1}) + \mathrm{j}U_1((-1)^k + \mathrm{e}^{-2\gamma 2_n h_1})]. \quad (32b)$$

The second term [. . .] on the right-side of equation (28) will produce $IB_{k,n}(-h_1)$. It is a great advantage that terms containing integrals over $q1'_m(x)q1_k(x)$ compensate each other. After some simple but lengthy manipulations one arrives at a linear, inhomogeneous system of equations ($k = 0, 1, 2, \ldots$) for the amplitudes A_m,

$$\sum_m A_m \left\{ -\delta_{m,k}\,\mathrm{e}^{-\gamma 1_k h_2} N1_k + \frac{\mathrm{j}}{2}\gamma 1_m h_1\,\mathrm{e}^{-\gamma 1_m h_2} \sum_n \frac{q2_n^2(h_2)}{\gamma 2_n h_2 N2_n}[\ldots]_{m,n} \right\}$$

$$= P_i\,\mathrm{e}^{+\gamma 1_\mu h_2}\left\{ \delta_{k,\mu} N1_\mu + \frac{\mathrm{j}}{2}\gamma 1_\mu h_1 \sum_n \frac{q2_n^2(h_2)}{\gamma 2_n h_2 N2_n}[\ldots]_{\mu,n} \right\}, \quad (33)$$

with the abbreviation

$$[\ldots]_{m,n} = \delta_{m,k}\frac{\gamma 2_n h_2 N1_k}{h_1 h_2(\gamma 2_n^2 + \varepsilon 1_m^2)} + \frac{q1_m(h_1)q1_k(h_1)}{4h_1^4(\gamma 2_n^2 + \varepsilon 1_m^2)(\gamma 2_n^2 + \varepsilon 1_k^2)}$$

$$\times [(\mathrm{j}U_1 + \gamma 2_n h_1) + (\mathrm{j}U_1 - \gamma 2_n h_1)(-1)^k \mathrm{e}^{-2\gamma 2_n h_1}]$$

$$\times \{(1 - (-1)^{m+k})(\gamma 2_n h_1 - \mathrm{j}U_1) + r_n(-1)^{m+k}$$

$$\times [(\mathrm{j}U_1 + \gamma 2_n h_1) + (\mathrm{j}U_1 - \gamma 2_n h_1)(-1)^m \mathrm{e}^{-2\gamma 2_n h_1}]\}, \quad (34)$$

and the Kronecker symbol $\delta_{m,k}$. The replacement $m \to \mu$ is applied in this term on the right-side of equation (33). With the solutions A_m from equation (33), $p_r(x, y)$ is computed from equation (25), $V_q(x_0)$ from equation (26) and then $p_t(x, y)$ and $p_s(x, y)$ from equations (23) and (24). All sound fields are known after that; the analytical task is solved. It is important to note for numerical computations that

the mode indices m (for the entrance duct) and n (for the exit duct) run over symmetrical and antisymmetrical modes. This is plausible, because the corner area is not symmetrical with respect to its central planes.

The final quantity for practical applications mostly will be the transmission loss of the corner. One could define it by the ratio of the effective transmitted power to the incident power, both computed in the respective end planes of the corner area. We shall see below in the numerical examples, however, that an important contribution—if not the most important contribution—to the transmission loss of the corner is localized *behind* the corner where the higher modes of the near field in the exit duct decay. It is, therefore, reasonable to measure the effect of the corner outside the near field zone: i.e., where only the least attenuated mode of the exit duct will remain. A good measure for the transmission loss of the duct corner, therefore, is the level difference of the least attenuated modes of both ducts, both levels measured at (or extrapolated to) the end planes of the ducts. But it shall be seen also that this measure becomes irrelevant, when the exit duct is rigid. Then the sum of the powers of the propagating modes in the exit duct should be applied.

The special situation of identical ducts, $G_1 = G_2 = G_3 = G$ and $h_1 = h_2$, does not lead to important simplifications in the computation, except that only one set of duct modes needs to be computed. In the numerical examples below, ducts are taken as "reference objects" with $h_1 = h_2 = 0{\cdot}2$ m, coated by layers of (locally reacting) mineral fibre absorbers $d_1 = d_2 = 0{\cdot}1$ m thick, with a flow resistivity of the porous absorber $\Xi_1 = \Xi_2 = 10$ kPa s/m^2. The thickness and/or resistivity will

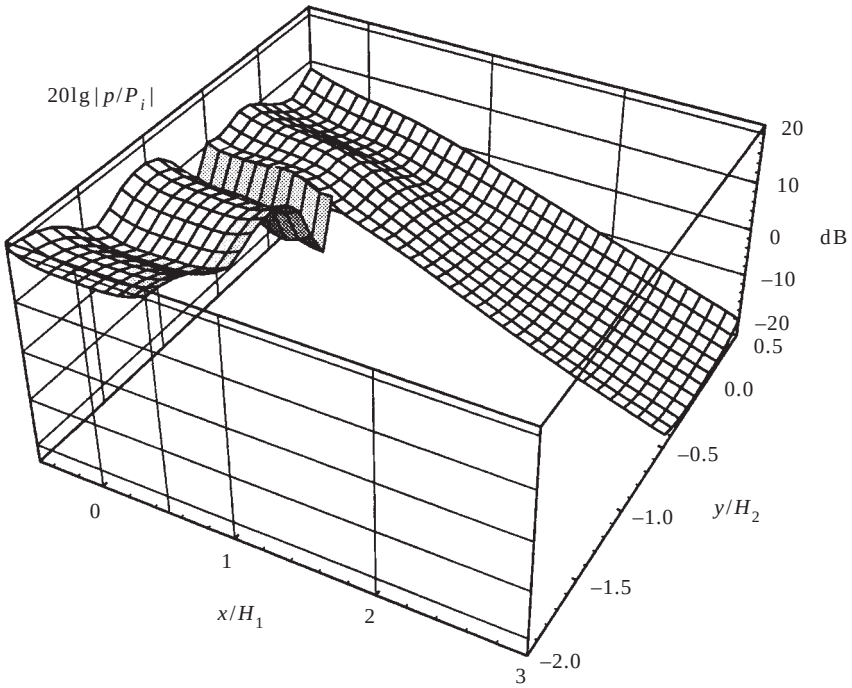

Figure 2. 3D-plot of the sound pressure level in an L-joint of lined ducts according to Figure 1(a); at $f = 500$ Hz. $\mu = 0$, $m_{hi} = 4$, $h_1 = h_2 = 0{\cdot}2$ m, $d_1 = d_2 = 0{\cdot}1$ m, $d_3 = 0{\cdot}2$ m, $\Xi_1 = \Xi_2 = 10$ kPa s/m^2, $\Xi_3 = 15$ kPa s/m^2.

be changed in some examples; the absorber layer will be covered by a resistive foil with a normalized series impedance Z_{si} in other examples. The admittances of the liners are computed by standard methods described in reference [13, Vol. II]. The mode orders will run up to m_{hi}, n_{hi} in both ducts. Numerical tests have shown that it is sufficient to take $m_{hi} = n_{hi} = 4$ with the dimensions and frequencies applied below; higher mode order limits (up to $m_{hi} = n_{hi} = 10$) modify the results only in details around the corners. Higher frequencies and/or wider ducts would need higher upper index limits.

Figure 2 shows a 3D-plot of the sound pressure $20 \lg |p(x, y)/P_i|$ in dB at $f = 500$ Hz for an arrangement as in Figure 1(a), plotted over x/H_1, y/H_2 with $H_i = 2h_i$. The ducts span over the interval $(-0{\cdot}5, 0{\cdot}5)$ in this representation. The ducts and the corner region are absorbing (see the list of parameters in the diagram). The sound field is steady (as its x-derivative) at the limit between zone III and zone II. It is steady—within the precision of the minimum square error principle introduced by equation (30)—also in the exit plane of the entrance duct; however, its slope in the y-direction has a jump, whereas the y-component of the particle velocity is steady too. This is plausible in the frame of the present theory. The relevant y-component of the field admittance changes in the exit plane of the entrance duct from the axial admittance of the modes in duct 1 into the lateral admittance in the corner area, i.e., into the lateral admittance of the modes in duct 2. It is this jump of the relevant field admittance which produces the reflection indicated by the standing wave in the entrance duct. The corresponding waviness continues somehow into the corner area, but there it is produced by the

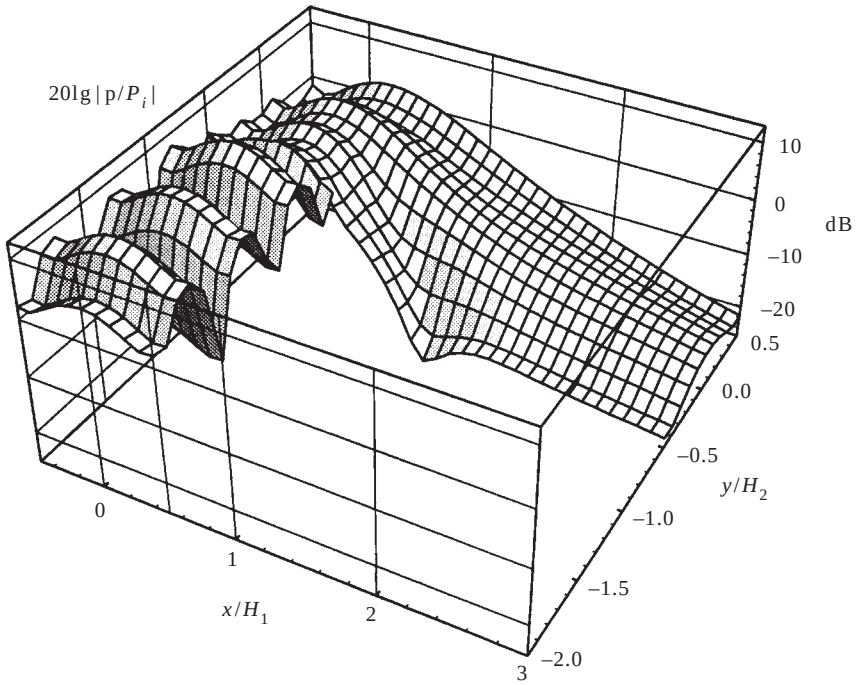

Figure 3. As Figure 2 but at $f = 1000$ Hz.

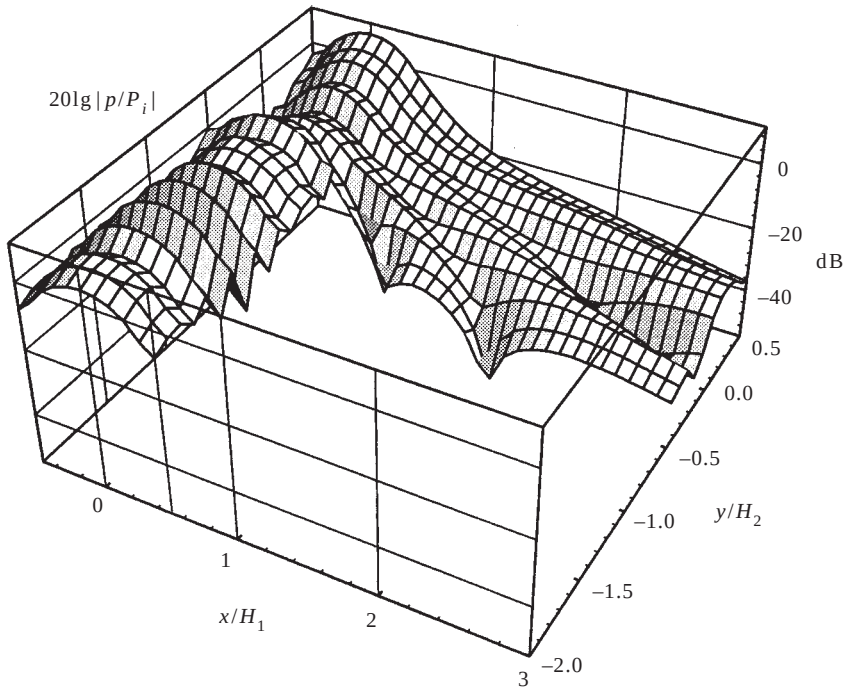

Figure 4. As Figure 2 but at $f = 2000$ Hz.

interference of a superposition of modes. The higher modes of the corner area have decayed in the exit duct after a distance of about $2H_2$; the lateral profile of the field is then stationary, it is the profile of the least attenuated mode. In Figure 3 the ducts are the same as before, only the frequency is doubled to $f = 1000$ Hz. The range of the near fields in duct 2 has extended, but the least attenuated mode is still dominant after a distance of about $2H_2$. In Figure 4 with a further increase in the frequency to $f = 2000$ Hz, the near field of the higher modes extends deeper into duct 2 than the shown range. This is important with respect to both measurements and application of the corner attenuation. If, for example, a splitter silencer is placed in the exit duct within the range of higher modes, then the excitation of that silencer will be at a still rather high level. In Figure 5 (at $f = 1000$ Hz), the front side wall of duct 2 is rigid, $G_3 = 0$, and the absorber of the ducts is covered with a resistive foil with $Z_{s2} = 1$, thereby reducing the attenuation in the ducts. The level in the exit duct at the end of the diagram has increased by about 6 dB as compared to that in Figure 3.

It was recommended above to characterize the transmission loss of the corner by the level difference of the least attenuated modes in both ducts at the end planes of the ducts. Figure 6 shows the sound pressure levels of these modes alone, but with the computation for the mode amplitudes including higher modes ($f = 1000$ Hz, both ducts and corner area absorbing). The level jump is placed at the exit plane of the entrance duct. This is a special feature (an artefact) of the

present theory; the place of the jump will change over to the entrance plane of the exit duct in the next section, and it will be distributed on both planes in the modal analysis in section 4. It is therefore not allowed to draw from this diagram the conclusion that the transmission loss of the corner is localized in the exit plane of the entrance duct.

The following diagrams show frequency response curves of the transmission loss of the corner $D = -20 \lg |p_{tv}(h_1 0)/p_{i\mu}(0, -h_2)|$ dB defined by the level difference of the least attenuated modes μ, v in the ducts at their end planes. In Figure 7 with absorbing ducts, the thickness d_3 of the porous layer of the corner absorber (with the admittance G_3) is changed. A value $d_3 = 0$ indicates a rigid corner wall. The precise value of the absorption coefficient of the corner absorber is evidently not very important. A rigid corner wall opposite the exit duct produces some interference variations of D corresponding to the interference pattern of the higher modes in the corner area. Figure 8 combines some situations of the absorption of the entrance duct and of the corner wall opposite the exit duct (this is always absorbing). The diagram shows that there exists some flexibility in the application of the transmission loss of a duct corner, depending on the frequency range in which one would like to enhance the attenuation. In Figure 9, it is tried to reduce the attenuation of the exit duct by the application of a resistive foil with a (normalized) series impedances Z_{s2} on the porous absorber layer (it will be explained in section 5 why rigid exit ducts cannot be treated by the theory of this

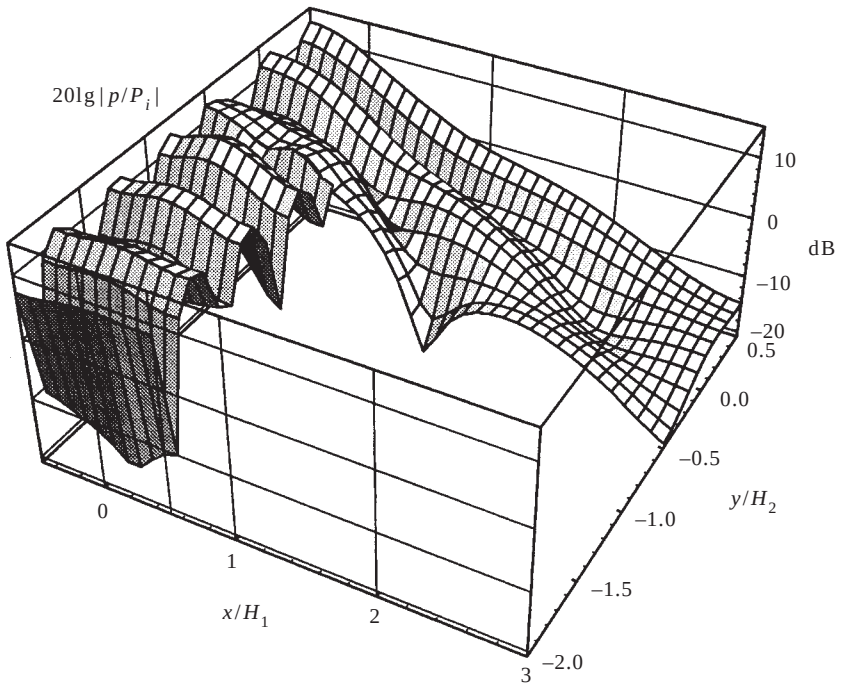

Figure 5. Sound pressure level in an L-joint of lined ducts according to Figure 1(a); at $f = 1000$ Hz as in Figure 3, but with a rigid corner wall and the absorber layer in duct 2 covered by a resistive foil. $\mu = 0$, $m_{hi} = 4$, $h_1 = h_2 = 0{\cdot}2$ m, $d_1 = d_2 = 0{\cdot}1$ m, $d_3 = 0{\cdot}2$ m, $Z_s = Z_{s2} = 1$, $\Xi_1 = \Xi_2 = 10$ kPa s/m^2.

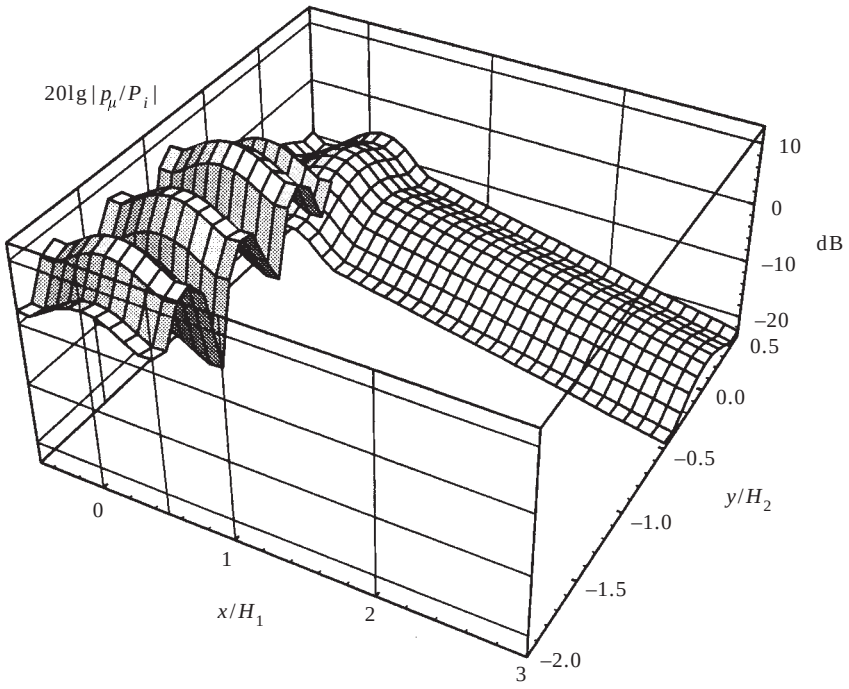

Figure 6. Sound pressure level in an L-joint of lined ducts according to Figure 1(a); at $f = 1000$ Hz as in Figure 3; however, only the level of the least attenuated mode is shown. Other parameters as Figure 3.

section). The new feature in this diagram is the appearance of a sharp dip of the transmission loss at the cut-on frequency of the first higher mode in the exit duct with low attenuation. This is quite plausible when it is understood that the transmission loss of the duct corner primarily is a matter of pattern matching of the field pattern in the corner area to the mode pattern in the exit duct. Figure 10 finally changes the duct width ratio h_1/h_2 (all surfaces absorbing). It is somewhat surprising at first glance that a narrow entrance duct produces a lower transmission loss at high frequencies than a wider duct. The explanation for this finding is that the number and strength of higher modes in the corner area is lower with a narrow entrance duct than with a wide entrance duct. This again indicates the role of the mode pattern in the corner area.

Figures 11(a, b) prepare for the comparison mentioned above between the theories of this and the following sections (Figure 11(a) with $f = 1000$ Hz; Figure 11(b) with $f = 2000$ Hz). The duct and corner linings are identical everywhere.

3. L-JOINT WITH ABSORBER OPPOSITE THE ENTRANCE DUCT

The arrangement now will be that of Figure 1(b). It corresponds better to the simple idea that a duct corner produces its transmission loss mainly by the

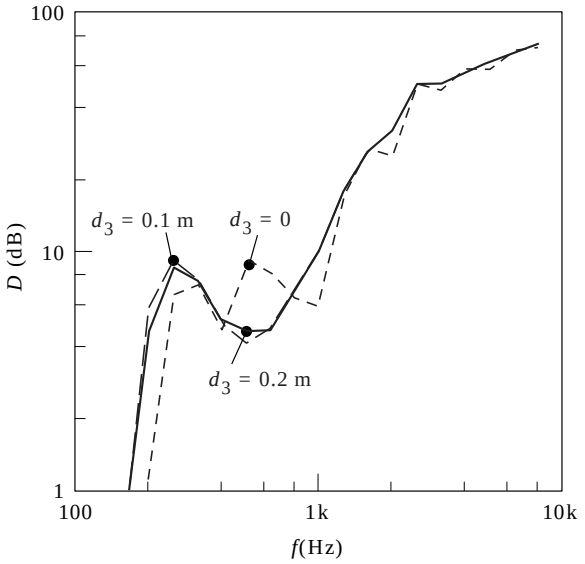

Figure 7. Frequency curves of the loss $D = 20 \lg |p_i(0, -h_2)/p_{t\mu}(h_1, 0)|$ of L-joints of lined ducts according to Figure 1(a); for three values of the layer thickness d_3 of the corner absorber.

absorption of the corner wall opposite the entrance duct. The present system—after an exchange of the h_i, G_i, $i = 1, 2$—is reciprocal to that of the previous section, if the incident wave comes from the duct $i = 2$. It could be computed therefore with the method of the previous section in combination with the principal of reciprocity for modes in duct branches, which was formulated by Cho [11].

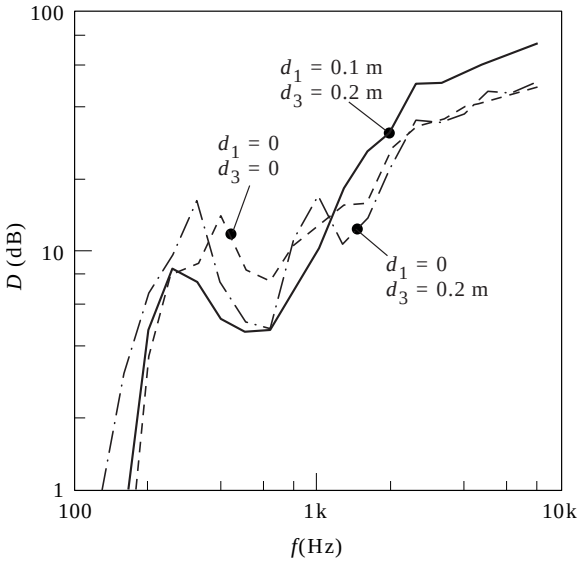

Figure 8. Frequency curves of the loss $D = 20 \lg |p_i(0, -h_2)/p_{t\mu}(h_1, 0)|$ of L-joints of lined ducts according to Figure 1(a), for different combinations of the absorption of the entrance duct and the corner absorber. Other parameters as Figure 2.

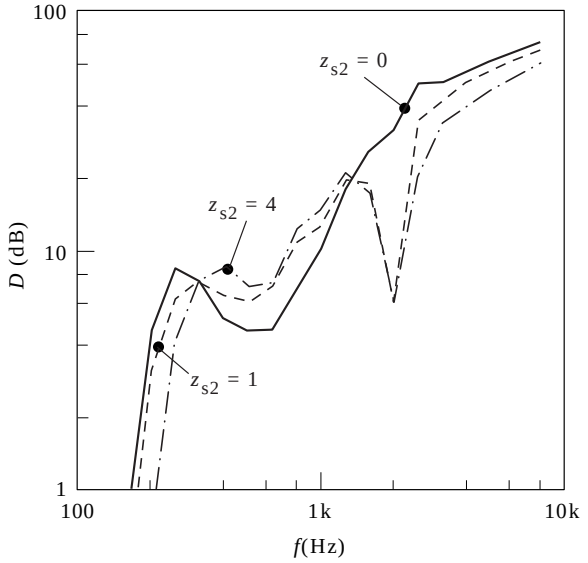

Figure 9. Frequency curves of the loss $D = 20 \lg |p_i(0, -h_2)/p_{t\mu}(h_1, 0)|$ of L-joints of lined ducts according to Figure 1(a); the attenuation of the exit duct is reduced by resistive foils with increasing (normalized) flow resistance Z_S. Other parameters as Figure 2.

Instead of this detour through the principle of reciprocity (it would be a detour, because the computations must be repeated for all mode orders of the incident mode in one duct which will be used in the synthesis of the field in the reciprocal exit duct), a direct way to a computation of the sound fields in the arrangement of Figure 1(b) will be derived. Now assume a fictitious velocity source $V_q(x_0, y_0)$ in the entrance plane of the exit duct $x_0 = h_1$, $y_0 = (-h_2, +h_2)$ (V_q is positive when

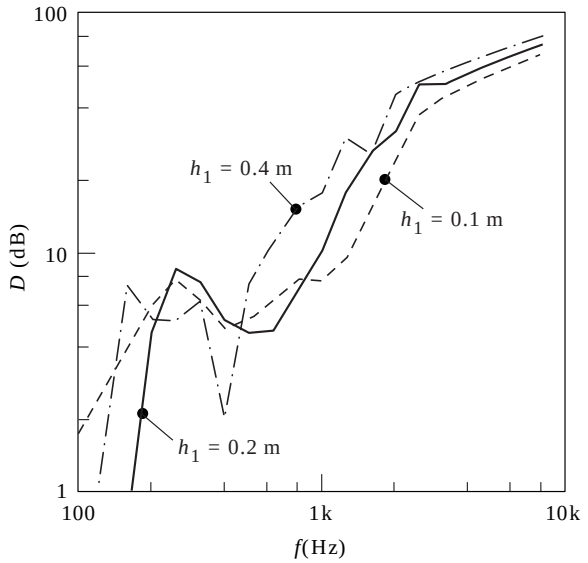

Figure 10. Frequency curves of the loss $D = 20 \lg |p_i(0, -h_2)/p_{t\mu}(h_1, 0)|$ of L-joints of lined ducts according to Figure 1(a), for different widths $2h_1$ of the entrance duct. Other parameters as Figure 2.

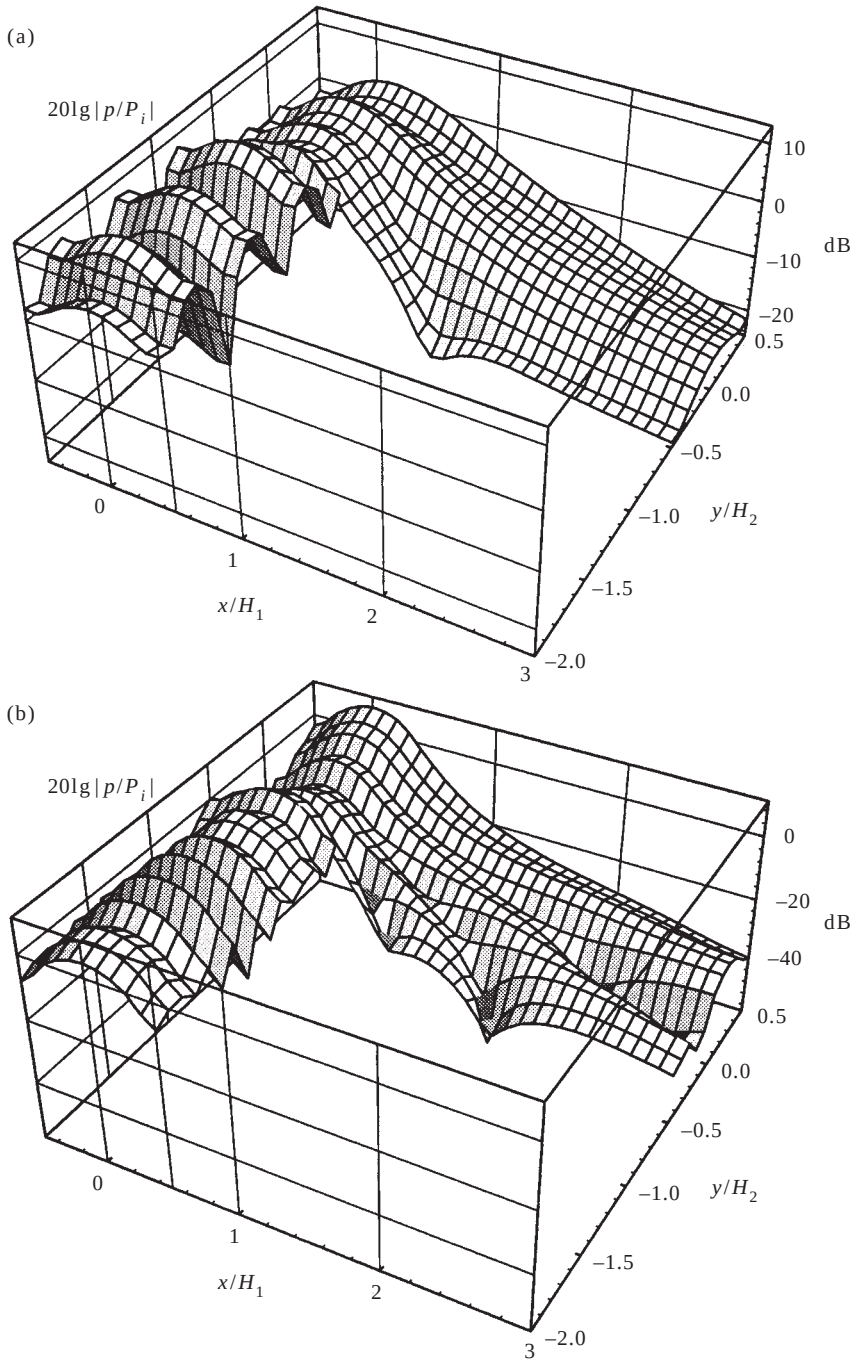

Figure 11. (a) 3D-plot of the sound pressure level in L-joints of lined ducts according to Figure 1(a), at $f = 1000$ Hz, with identical lining everywhere; to be compared to results of later sections. $\mu = 0$, $m_{hi} = 4$, $h_1 = h_2 = 0{\cdot}2$ m, $d_1 = d_2 = d_3 = 0{\cdot}1$ m, $\Xi_1 = \Xi_2 = \Xi_3 = 10$ kPa s/m^2. (b) as (a) but at $f = 2000$ Hz.

directed into the corner area). Start with $p_i + p_r$ in composing the field in zones I and III, with p_i again the incident mode with order μ from the entrance duct, and p_r now the reflection of this mode at the surface of the corner absorber with the surface admittance G_3. This would be the complete field in zones I and III, if the lining of duct 1 (and the outer wall) would extend over the entrance plane of the exit duct (a situation which is indicated in grey in Figure 1(b)). The opening of duct 2 will produce an additional scattered field p_s in zones I and III. It shall be generated by a fictitious source V_q. The scattered field p_s can be taken as a function of V_q (with evident exchanges of the symbols) from the previous section. The boundary conditions at the limit between zones I and III are satisfied by the field $p_i + p_r + p_s$. Then the boundary conditions at the entrance plane of the exit duct can be formulated in which it is assumed that the transmitted field p_t, is the sum of modes with amplitudes D_n. This will lead to a linear, inhomogeneous system of equations for the D_n.

The sound fields in zones I and III consist of $p(x, y) = p_i(x, y) + p_r(x, y) + p_s(x, y)$. The sound field in zone II is $p(x, y) = p_t(x, y)$. The formulations

$$p_i(x, y) = P_i q1_\mu(x)\, \mathrm{e}^{-\gamma 1_\mu y},$$

$$p_r(x, y) = P_i r_\mu q1_\mu(x)\, \mathrm{e}^{+\gamma 1_\mu (y - 2h_2)} = P_i R_\mu q1_\mu(x)\, \mathrm{e}^{+\gamma 1_\mu y},$$

$$p_t(x, y) = \sum_n D_n q2_n(y)\, \mathrm{e}^{-\gamma 2_n (x - h_1)}. \tag{35}$$

are made. Therein

$$r_m = (\mathrm{j}\gamma 1_m/k_0 + Z_0 G_3)/(\mathrm{j}\gamma 1_m/k_0 - Z_0 G_3) \tag{36}$$

are the modal reflection factors at the surface of the corner absorber with the surface admittance G_3. $R_m = r_m\, \mathrm{e}^{-2\gamma 1_m h_2}$ are the modal reflection factors "measured" in the co-ordinate plane $y = 0$. The amplitudes D_n of the scattered wave are "defined" in the plane $x = h_1$.

One obtains, in analogy to the previous section (see equation (18)), for the contribution of the volume source element $V_q(x_0, y_0)\, \mathrm{d}y_0$ to the scattered field p_s (with $x_0 = h_1,\ y_0 = (-h_2, +h_2)$),

$$\mathrm{d}p_s(x, y) = \mathrm{j}\, \frac{k_0 Z_0}{4}\, V_q(x_0, y_0)\, \mathrm{d}y_0 \sum_m \frac{q1_m(h_1) q1_m(x)}{\gamma 1_m h_1 N1_m} [\mathrm{e}^{\pm \gamma 1_\mathrm{m}(y - y_0)} + \mathrm{R_m}\, \mathrm{e}^{+\gamma 1_m (y + y_0)}],$$

$$\begin{Bmatrix} y < y_0 \\ y > y_0 \end{Bmatrix}. \tag{37}$$

The scattered field p_s follows by integration:

$$p_s(x, y) = \frac{k_0 h_2 Z_0}{2} \sum_m \frac{q1_m(h_1) q1_m(x)}{\gamma 1_m h_1 N 1_m}$$

$$\times \begin{Bmatrix} e^{+\gamma 1_m y}[IB_m(-h_2) + R_m IA_m(h_2)], & y < -h_2 \\ e^{+\gamma 1_m y}[IB_m(y) + R_m IA_m(h_2)] + e^{-\gamma 1_m y} IA_m(y), & -h_2 < y < h_2 \end{Bmatrix}, \quad (38)$$

with the integrals

$$IA_m(y) = \frac{j}{2h_2} \int_{-h_2}^{y} e^{+\gamma 1_m y_0} V_q(y_0)\, dy_0, \quad IB_m(y) = \frac{j}{2h_2} \int_{y}^{h_2} e^{-\gamma 1_m y_0} V_q(y_0)\, dy_0. \quad (39)$$

The analysis up to here broadly follows the analysis of the previous section. The main difference will be introduced by the formulation and application of the boundary conditions in the entrance plane of the exit duct. The boundary condition for the particle velocity (in the x-direction) is now

$$v_{tx}(x_0, y_0) \overset{!}{=} -V_q(x_0, y_0) + G_1(p_i(x_0, y_0) + p_r(x_0, y_0)). \quad (40)$$

It describes the fact that $V_q = 0$ when the lining and the outer wall of duct 1 would cover the opening of duct 2, because then v_{tx} is the velocity at the surface of the lining. From equation (40) one gets by insertion of equation (35),

$$V_q(h_1, y_0) = V_q(y_0) = \frac{j}{k_0 h_2 Z_0} \sum_n D_n \gamma 2_n h_2 q2_n(y_0)$$

$$+ P_i \frac{U_1}{k_0 h_1 Z_0} q1_\mu(h_1)[e^{-\gamma 1_\mu y_0} + R_\mu e^{+\gamma 1_\mu y_0}] \quad (41)$$

(see equation (4) for U_1). The sound pressure boundary condition $p_i(x_0, y_0) + p_r(x_0, y_0) + p_s(x_0, y_0) \overset{!}{=} p_t(x_0, y_0)$ at $x = x_0 = h_1$ reads

$$p_s(h_1, y_0) = \sum_n D_n q2_n(y_0) - P_i q1_\mu(h_1)[e^{-\gamma 1_\mu y_0} + R_\mu e^{+\gamma 1_\mu y_0}]. \quad (42)$$

If, on the other hand, one inserts V_q from equation (41) into equations (38) and (39), the integrals $IA_m(y)$, $IB_m(y)$ take the forms

$$IA_m(y) = P_i \frac{jU_1}{k_0 h_1 Z_0} q1_\mu(h_1)[I1_m(y) + R_\mu I3_m(y)] + \frac{j}{k_0 h_2 Z_0} \sum_n D_n \gamma 2_n h_2 IA_{m,n}(y),$$

$$IB_m(y) = P_i \frac{jU_1}{k_0 h_1 Z_0} q1_\mu(h_1)[I2_m(y) + R_\mu I4_m(y)] + \frac{j}{k_0 h_2 Z_0} \sum_n D_n \gamma 2_n h_2 IB_{m,n}(y), \quad (43)$$

with the abbreviations

$$IA_{m,n}(y) := \frac{\mathrm{j}}{2h_2} \int_{-h_2}^{y} \mathrm{e}^{+\gamma 1_m y_0} q2_n(y_0)\, \mathrm{d}y_0 := Ia_{m,n}(y) - Ia_{m,n}(-h_2),$$

$$IB_{m,n}(y) := \frac{\mathrm{j}}{2h_2} \int_{y}^{h_2} \mathrm{e}^{-\gamma 1_m y_0} q2_n(y_0)\, \mathrm{d}y_0 := Ib_{m,n}(h_2) - Ib_{m,n}(y), \tag{44}$$

and the indefinite integrals

$$Ia_{m,n}(y) := \frac{1}{2h_2} \int^{y} \mathrm{e}^{+\gamma 1_m y_0} q2_n(y_0)\, \mathrm{d}y_0 = \frac{\mathrm{e}^{\gamma 1_m y}}{2h_2(\gamma 1_m^2 + \varepsilon 2_n^2)} [\gamma 1_m q2_n(y) - q2_n'(y)],$$

$$Ib_{m,n}(y) := \frac{1}{2h_2} \int^{y} \mathrm{e}^{-\gamma 1_m y_0} q2_n(y_0)\, \mathrm{d}y_0 = \frac{-\mathrm{e}^{-\gamma 1_m y}}{2h_2(\gamma 1_m^2 + \varepsilon 2_n^2)} [\gamma 1_m q2_n(y) + q2_n'(y)]. \tag{45}$$

These become at the intervals limits (together with equation (5))

$$Ia_{m,n}(h_2) = \frac{\mathrm{e}^{\gamma 1_m h_2} q2_n(h_2)}{2h_2^2(\gamma 1_m^2 + \varepsilon 2_n^2)} [\gamma 1_m h_2 + \mathrm{j}U_2],$$

$$Ia_{m,n}(-h_2) = (-1)^n \frac{\mathrm{e}^{-\gamma 1_m h_2} q2_n(h_2)}{2h_2^2(\gamma 1_m^2 + \varepsilon 2_n^2)} [\gamma 1_m h_2 - \mathrm{j}U_2],$$

$$Ib_{m,n}(h_2) = -\frac{\mathrm{e}^{-\gamma 1_m h_2} q2_n(h_2)}{2h_2^2(\gamma 1_m^2 + \varepsilon 2_n^2)} [\gamma 1_m h_2 - \mathrm{j}U_2] = (-1)^{n+1} Ia_{m,n}(-h_2),$$

$$Ib_{m,n}(-h_2) = (-1)^{n+1} \frac{\mathrm{e}^{\gamma 1_m h_2} q2_n(h_2)}{2h_2^2(\gamma 1_m^2 + \varepsilon 2_n^2)} [\gamma 1_m h_2 + \mathrm{j}U_2] = (-1)^{n+1} Ia_{m,n}(h_2). \tag{46}$$

The other integrals in equation (43),

$$I1_m(y) := \frac{1}{2h_2} \int_{-h_2}^{y} \mathrm{e}^{(\gamma 1_m - \gamma 1_\mu) y_0}\, \mathrm{d}y_0, \quad I3_m(y) := \frac{1}{2h_2} \int_{-h_2}^{y} \mathrm{e}^{(\gamma 1_m + \gamma 1_\mu) y_0}\, \mathrm{d}y_0,$$

$$I2_m(y) := \frac{1}{2h_2} \int_{y}^{h_2} \mathrm{e}^{-(\gamma 1_m + \gamma 1_\mu) y_0}\, \mathrm{d}y_0, \quad I4_m(y) := \frac{1}{2h_2} \int_{y}^{h_2} \mathrm{e}^{-(\gamma 1_m - \gamma 1_\mu) y_0}\, \mathrm{d}y_0, \tag{47}$$

can be easily evaluated. It should be mentioned only that $I1_m$, $I4_m$ for $m = \mu$ have the limit values

$$I1_\mu(y) = \tfrac{1}{2}(1 + y/h_2), \quad I4_\mu(y) = \tfrac{1}{2}(1 - y/h_2). \tag{48}$$

After these preparations p_s in zone I can be written as

$$p_s(x, y) = \tfrac{1}{2} \sum_m \frac{q1_m(h_1) q1_m(x)}{\gamma 1_m h_1 N 1_m} \, \mathrm{e}^{+\gamma 1_m y}$$

$$\times \left\{ P_i U_1 \frac{h_2}{h_1} \, q1_\mu(h_1) \left[(1 + R_m R_\mu) \frac{\sinh((\gamma 1_m + \gamma 1_\mu) h_2)}{(\gamma 1_m + \gamma 1_\mu) h_2} \right.\right.$$

$$\left. + (R_m + R_\mu) \frac{\sinh((\gamma 1_m - \gamma 1_\mu) h_2)}{(\gamma 1_m - \gamma 1_\mu) h_2} \right]$$

$$\left. + \mathrm{j} \sum_n D_n \gamma 2_n h_2 ((-1)^n + R_m)(Ia_{m,n}(h_2) - Ia_{m,n}(-h_2)) \right\}, \qquad (49a)$$

and p_s in zone III as:

$$p_s(x, y) = \tfrac{1}{2} \sum_m \frac{q1_m(h_1) q1_m(x)}{\gamma 1_m h_1 N 1_m}$$

$$\times \left\{ P_i U_1 \frac{h_2}{h_1} \, q1_\mu(h_1) [[\mathrm{e}^{+\gamma 1_m y} [I2_m(y) + R_m (I1_m(h_2) + R_\mu I3_m(h_2))\right.$$

$$+ R_\mu I4_m(y)] + \mathrm{e}^{-\gamma 1_m y} [I1_m(y) + R_\mu I3_m(y)]]]$$

$$+ \mathrm{j} \sum_n D_n \gamma 2_n h_2 [[\mathrm{e}^{+\gamma 1_m y} [-Ib_{m,n}(y) + R_m Ia_{m,n}(h_2) - ((-1)^n + R_m)$$

$$\left. \times Ia_{m,n}(-h_2)] + \mathrm{e}^{-\gamma 1_m y} [Ia_{m,n}(y) - Ia_{m,n}(-h_2)]] \right\}. \qquad (49b)$$

If one introduces equation (49b) (after $y \to y_0$) into the left-side of equation (42) and then applies on both sides the orthogonality integral operator

$$\frac{1}{2h_2} \int_{-h_2}^{h_2} \ldots q2_k(y_0) \, \mathrm{d}y_0, \qquad (50)$$

simple but longer transformations lead to the linear, inhomogeneous system of equations ($k = 0, 1, 2, \ldots$) for the D_n:

$$D_k N2_k - \frac{\mathrm{j}}{2}\sum_n D_n \gamma 2_n h_2 \sum_m \frac{q1_m^2(h_1)}{\gamma 1_m h_1 N1_m}$$

$$\times \left[\delta_{n,k}\frac{h_2}{h_1}\frac{\gamma 1_m h_1 N2_k}{h_2^2(\gamma 1_m^2 + \varepsilon 2_k^2)} - Ia_{m,n}(-h_2)((-1)^n IA_{m,k}(h_2) + IB_{m,k}(-h_2))\right.$$

$$\left. + R_m IA_{m,n}(h_2) IA_{m,k}(h_2)\right]$$

$$= P_i q1_\mu(h_1)\left\{IB_{\mu,k}(-h_2) + R_\mu IA_{\mu,k}(h_2) + \frac{1}{2}U_1\frac{h_2}{h_1}\sum_m \frac{q1_m^2(h_1)}{\gamma 1_m h_1 N1_m}\right.$$

$$\times \left[\left[\frac{IB_{\mu,k}(-h_2) + R_\mu IA_{\mu,k}(h_2)}{2h_2(\gamma 1_m + \gamma 1_\mu)} + IA_{m,k}(h_2)\right.\right.\left[R_m(I1_m(h_2) + R_\mu I3_m(h_2))\right.$$

$$\left.\left. - \frac{\mathrm{e}^{-(\gamma 1_m + \gamma 1_\mu)h_2}}{2h_2(\gamma 1_m + \gamma 1_\mu)}\right] - R_\mu IB_{m,k}(-h_2)\frac{\mathrm{e}^{-(\gamma 1_m + \gamma 1_\mu)h_2}}{2h_2(\gamma 1_m + \gamma 1_\mu)}\right.$$

$$+ \frac{IB_{\mu,k}(-h_2) - IB_{m,k}(-h_2)\,\mathrm{e}^{-(\gamma 1_m - \gamma 1_\mu)h_2}}{2h_2(\gamma 1_m - \gamma 1_\mu)}$$

$$\left.\left. + R_\mu\frac{IA_{\mu,k}(h_2) - IA_{m,k}(h_2)\,\mathrm{e}^{-(\gamma 1_m - \gamma 1_\mu)h_2}}{2h_2(\gamma 1_m - \gamma 1_\mu)}\right]\right]\right\}. \tag{51}$$

For $m \to \mu$ the last two terms go over to $IB_{\mu,k}(-h_2)/2$ and $R_\mu IA_{\mu,k}(h_2)/2$, respectively. When the solutions D_n of this system are known, the fields p_t follow from equation (35) and p_s from equation (49). The task then is solved analytically; all fields are known. Numerical tests have shown that the upper limit m_{hi} of the mode orders m, n, k can be kept rather low. A limit $m_{hi} = 4$ is sufficient for the frequency and duct width parameters used below. Again the numerical computations are restricted to the (most important) case of the least attenuated mode of duct 1 as incident wave; it is the mode $\mu = 0$ for our parameters of the ducts and linings (under some conditions, it can become the mode $\mu = 2$).

The presentation of examples begins with the counterparts of Figure 11 in Figures 12(a, b) with equal ducts and linings everywhere. The theories on which these diagrams are based are approximate, as explained in the introduction. Corresponding diagrams differ from each other in the near fields of the corner area within about ± 2 dB. The agreement is better in the far fields in the ducts. Both theories can thus be applied for the computation of transmission loss measures which are defined by far fields. Figure 13 shows the transmission loss according

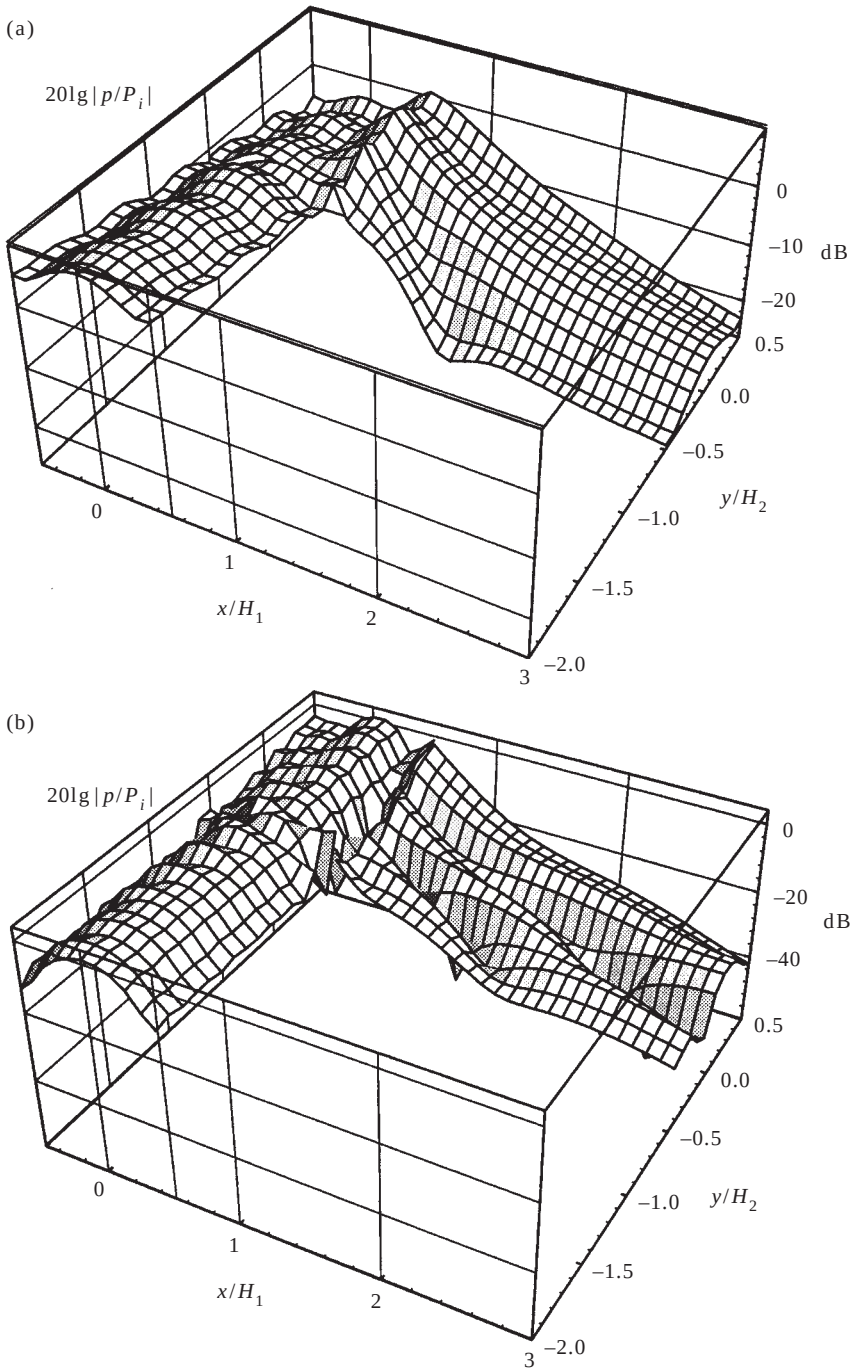

Figure 12. (a) 3D-plot of the sound pressure level in L-joints of lined ducts according to Figure 1(b), at $f = 1000$ Hz, with identical lining everywhere; to be compared to Figure 11(a) of section 2. Other parameters as Figure 11. (b) As (a) but at $f = 2000$ Hz, to be compared to Figure 11(b) of section 2.

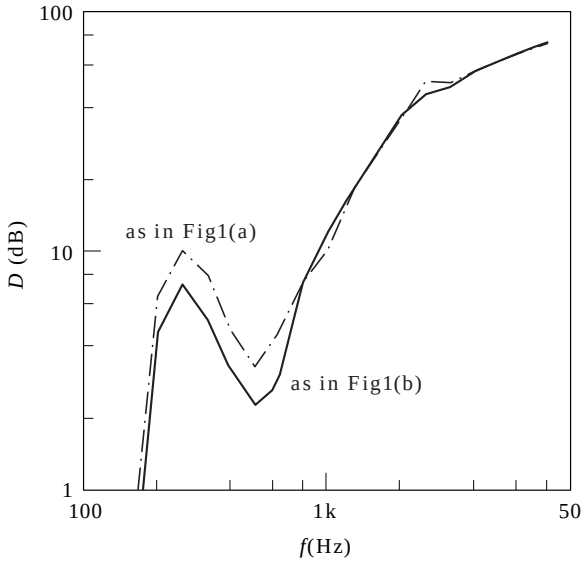

Figure 13. Frequency curves of the loss $D = 20 \lg |p_i(0, -h_2)/p_{tu}(h_1, 0)|$ of L-joints of lined ducts according to Figures 1(a) and 1(b), with identical lining everywhere, corresponding to Figures 11 and 12.

to both theories. The agreement is sufficient for high frequencies. The difference at lower frequencies comes from the fact that there the fundamental modes in both ducts are dominant and therefore influenced by the details of the field matching.

A higher precision can be attributed to the results of this section. This can be concluded from the fact that the field formulation here explicitly contains the wave reflected at G_3 and thus more information about the field structure, and this conclusion, is supported both by a critical inspection of results from both theories as well as from comparisons made with results of the following section.

The exit duct of Figure 14 is nearly rigid (thin absorber layer covered by a resistive foil with high flow resistance); the corner absorber with the admittance G_3 is highly absorbent. The level values of the diagram in the exit duct indicate only a low transmission loss of the corner as compared to absorbing exit ducts. This should be kept in mind when in later diagrams frequency response curves of the corner transmission loss for (nearly) rigid exit ducts will be shown; they will indicate high losses (based on the level difference of the least attenuated modes) with rigid exit ducts also. The solution of this discrepancy can be seen from Figure 14: the field in the exit duct there evidently is composed mainly of higher propagating modes. The fundamental mode is weak, giving high computational loss values, but the real losses are low, due to the power in the propagating higher modes. The philosophy of the transmission loss based on the least attenuated mode loses its basis for (nearly) rigid exit ducts. The sum of the modal powers should be applied in this case. In Figure 15, not only the exit duct is (nearly) rigid, but also the wall opposite duct 1. The field in the exit duct here also consists of higher modes, with a different mode mixture, however.

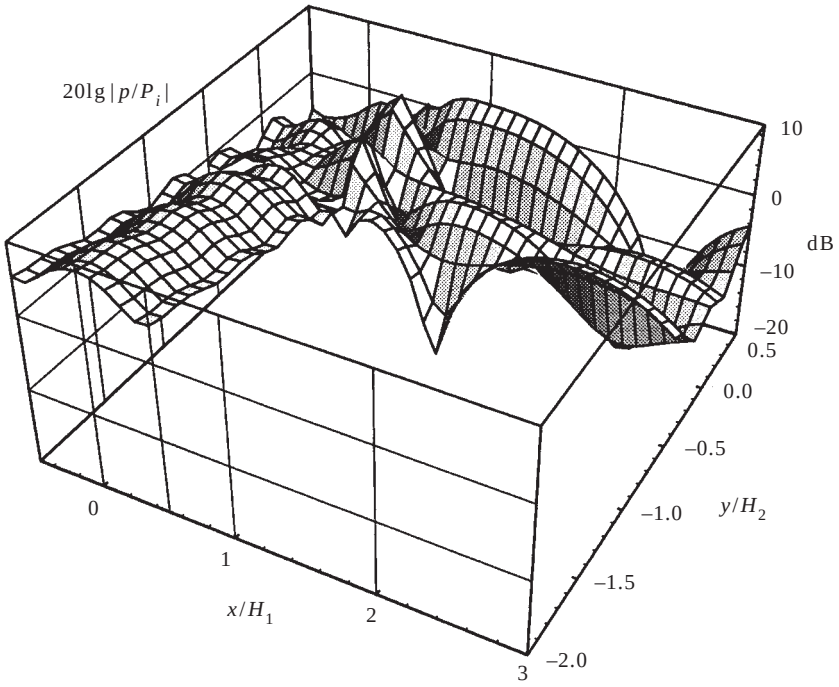

Figure 14. 3D-plot of the sound pressure level in L-joints of lined ducts according to Figure 1(b), at $f = 1000$ Hz; the corner opposite duct 1 is highly absorbent, the exit duct is approximately rigid, $\mu = 0$, $m_{hi} = 4$, $h_1 = h_2 = 0{\cdot}2$ m, $d_1 = 0{\cdot}1$ m, $d_2 = 0{\cdot}01$ m, $d_3 = 0{\cdot}2$ m, $\Xi_1 = \Xi_2 = 10$ kPa s/m^2, $\Xi_3 = 15$ kPa s/m^2, $Z_{S2} = 10$.

The exit duct for Figure 16 is again absorbing; the entrance duct is approximately and the corner side exactly rigid. A strong standing wave pattern exists in the corner area. It excites corresponding higher modes in the exit duct. These, however, decay quickly in the near field range of this duct, so that only the least attenuated mode on the lower level remains after a short distance from the duct entrance. Figure 17 helps to estimate the potential effect of resonator absorbers as coatings for the duct corner. Both ducts are absorbing, the corner absorber is extremely soft ($Z_0 G_3 = 1000$). One can see the low level in front of the absorber as a consequence of the soft reflection which compensates the incident wave. A heuristic idea could be, that the compensation due to the soft reflection would extend far into the corner area and thus the excitation of the exit duct should be low. The compensation in Figure 17 is, however, effective only immediately in front of the corner absorber, as can be seen from the low levels. The level is again rather high in places deeper in the corner area, partially because of the finite propagation attenuation in that area, but mainly due to the scattered field from the exit duct.

Figure 18 contains frequency curves of the transmission loss (based on the level difference of the least attenuated modes) for different absorption of the corner absorber, absorbing (full line), rigid (dashed line), and soft (dash-pointed line). All states of the corner side wall produce high values of the transmission loss at high frequencies (with absorbing ducts). The soft wall also generates a relatively small

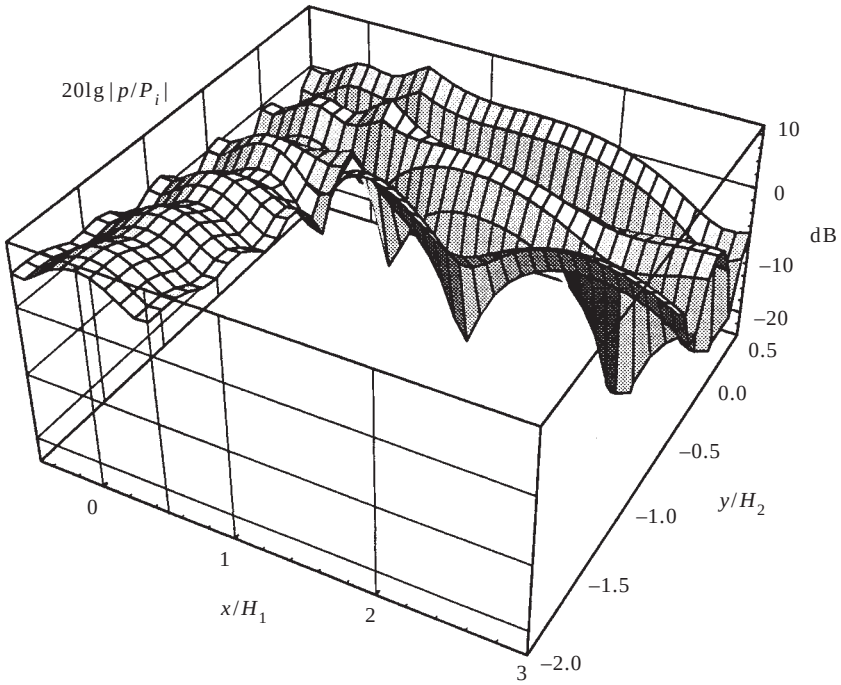

Figure 15. 3D-plot of the sound pressure level in L-joints of lined ducts according to Figure 1(b), at $f = 1000$ Hz; the corner opposite duct 1 is rigid, the exit duct is approximately rigid. Other parameters as Figure 14.

transmission loss at low frequencies (followed by a broad minimum at medium frequencies); the soft compensation there is effective over a wider range in the corner area. Figure 19 combines frequency curves of the transmission loss of absorbing and (nearly) rigid exit ducts and for absorbing and rigid corner walls. As it was stated above, the high values of the computed transmission loss with rigid exit ducts are misleading; the effective transmission loss is low due to propagating higher modes.

4. MODAL ANALYSIS OF A CORNER JOINT WITH TWO CORNER ABSORBERS

The analytical procedure in this section shall be explained with the graph of Figure 20. Now, two corner absorbers with the surface admittances G_3, G_4 at the corner walls are assumed; G_3 being opposite the exit duct, G_4 opposite the entrance duct. When the corner absorbers (and their rigid back terminations) are mirror reflected with respect to the central planes of the ducts (indicated in grey in Figure 20), one gets two new (fictitious) lined duct sections $i = 3, 4$ having widths $2h_3 = 2h_1$ and $2h_4 = 2h_2$ lined with absorbers of a surface admittance G_3, G_4, respectively. The modes in each of the sections are orthogonal to each other and form a set of functions suited for the synthesis of sound pressure profiles normal to the section axis (with the mode orders α, β below, representing symmetrical and

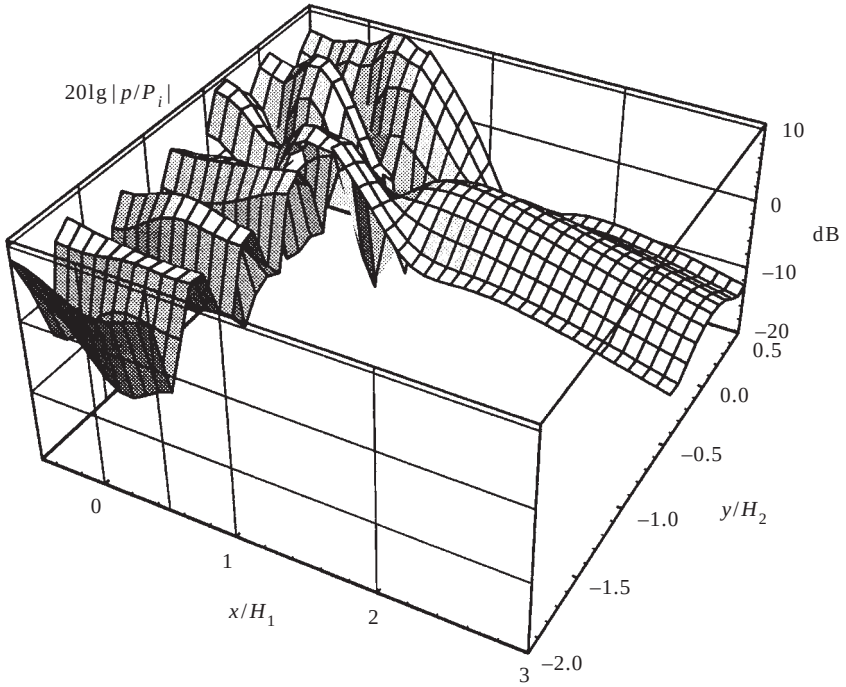

Figure 16. 3D-plot of the sound pressure level in L-joints of lined ducts according to Figure 1(b), at $f = 1000$ Hz; the corner opposite duct 1 is rigid, the entrance duct is approximately rigid, and the exit duct is absorbing. Other parameters as Figure 14.

anti-symmetrical modes). In each of the sections, a sum p_{si} of forward and backward propagating modes is assumed, where the backward running components are generated by reflection of the forward running components at the surface of the corner absorber which terminates the section (e.g., at G_4 in the section $i = 3$).

The fields in the ducts and in the corner area are formulated by

$$P_I(x, y) = p_i(x, y) + p_r(x, y), \qquad P_{II}(x, y) = p_t(x, y),$$
$$P_{III}(x, y) = p_{s3}(x, y) + p_{s4}(x, y), \tag{52}$$

with the components in the forms

$$p_i(x, y) = P_i q1_\mu(x)\, \mathrm{e}^{-\gamma 1_\mu (y + h_2)}, \qquad p_r(x, y) = \sum_m A_m q1_m(x)\, \mathrm{e}^{+\gamma 1_\mu (y + h_2)}, \tag{53, 54}$$

$$p_t(x, y) = \sum_n D_n q2_n(y)\, \mathrm{e}^{-\gamma 2_n (x - h_1)}, \tag{55}$$

$$p_{s3}(x, y) = \sum_\alpha B_\alpha q3_\alpha(x)[\mathrm{e}^{-\gamma 3_\alpha (y + h_2)} + R_\alpha\, \mathrm{e}^{-\gamma 3_\alpha (y + h_2)}], \tag{56}$$

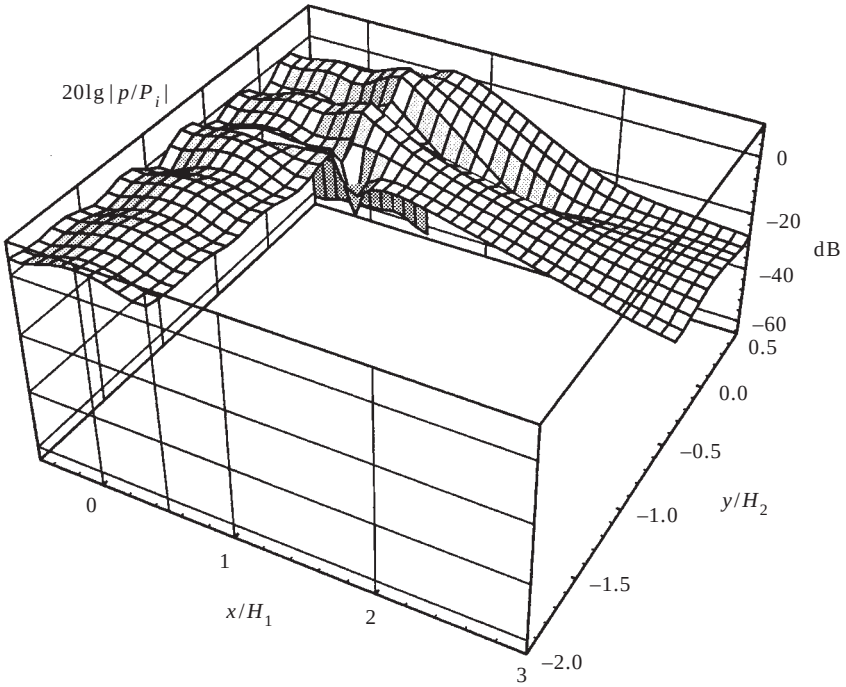

Figure 17. 3D-plot of the sound pressure level in L-joints of lined ducts according to Figure 1(b), at $f = 1000$ Hz; the corner opposite duct 1 is approximately pressure release, and the ducts are absorbing. $Z_0G_3 = 1000$. Other parameters as Figure 14.

$$p_{s4}(x, y) = \sum_{\beta} C_\beta q4_\beta(y)[\mathrm{e}^{+\gamma 4_\beta(x-h_1)} + R_\beta\, \mathrm{e}^{-\gamma 4_\beta(x-h_1)}]. \tag{57}$$

The $R_{\alpha,\beta}$ are the modal reflection factors in the sections $i = 3, 4$ "measured" in the end planes of the ducts. They follow from the reflection factors $r_{\alpha,\beta}$ at the admittances by

$$R_\alpha = r_\alpha\, \mathrm{e}^{-4\gamma 3_\alpha h_2}, \qquad r_\alpha = \frac{\mathrm{j}\gamma 3_\alpha/k_0 + Z_0G_4}{\mathrm{j}\gamma 3_\alpha/k_0 - Z_0G_4} = \frac{\mathrm{j}\gamma 3_\alpha h_2 + U_4}{\mathrm{j}\gamma 3_\alpha h_2 - U_4},$$

$$R_\beta = r_\beta\, \mathrm{e}^{-4\gamma 4_\beta h_1}, \qquad r_\beta = \frac{\mathrm{j}\gamma 4_\beta/k_0 + Z_0G_3}{\mathrm{j}\gamma 4_\beta/k_0 - Z_0G_3} = \frac{\mathrm{j}\gamma 4_\beta h_1 + U_3}{\mathrm{j}\gamma 4_\beta h_1 - U_3}. \tag{58}$$

The mode amplitudes A_m, B_α are defined in the end plane $y = -h_2$ of the entrance duct, and D_n, C_β are defined in the end plane $x = h_1$ of the exit duct.

The modes in all duct sections $i = 1$ to 4 have the shape of equation (1) with the profiles of equation (2); they satisfy the wave equation together with equations (3) and have the characteristic equation (4), and obey the relations (5). Each of the modes of the sections $i = 3, 4$ satisfies the conditions at the outer boundaries of the corner area, on one side by their character as section mode, on the other side by the formulation of the reflection factors. So the third of equations (52) obeys the boundary conditions at the real limitations of the corner area. The boundary conditions of field fitting by pressure and axial particle velocity must still be formulated.

The boundary condition for the sound pressure in the orifice of duct 1 is

$$P_i q1_\mu(x) + \sum_m A_m q1_m(x)$$

$$\stackrel{!}{=} \sum_\alpha B_\alpha q3_\alpha(x)(1 + R_\alpha) + \sum_\beta C_\beta q4_\beta(-h_2)(\mathrm{e}^{+\gamma 4_\beta(x-h_1)} + R_\beta\, \mathrm{e}^{-\gamma 4_\beta(x-h_1)}), \quad (59a)$$

and for the particle velocity

$$-P_i \gamma 1_\mu q1_\mu(x) + \sum_m A_m \gamma 1_m q1_m(x)$$

$$\stackrel{!}{=} -\sum_\alpha B_\alpha \gamma 3_\alpha q3_\alpha(x)(1 - R_\alpha) + \sum_\beta C_\beta q'4_\beta(-h_2)(\mathrm{e}^{+\gamma 4_\beta(x-h_1)} + R_\beta\, \mathrm{e}^{-\gamma 4_\beta(x-h_1)}). \quad (59b)$$

The corresponding boundary conditions in the entrance plane of duct 2 are

$$\sum_m D_n q2_n(y)$$

$$\stackrel{!}{=} \sum_\alpha B_\alpha q3_\alpha(h_1)(\mathrm{e}^{-\gamma 3_\alpha(y+h_2)} + R_\alpha\, \mathrm{e}^{+\gamma 3_\alpha(y+h_2)}) + \sum_\beta C_\beta q4_\beta(y)(1 + R_\beta), \quad (60a)$$

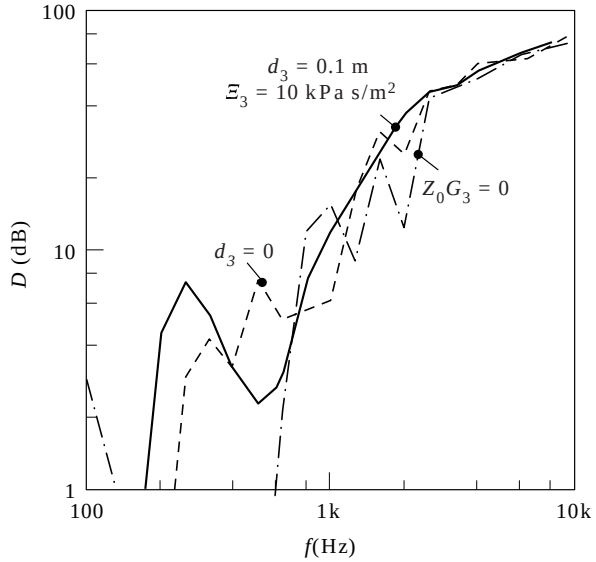

Figure 18. Frequency curves of the loss $D = 20 \lg |p_i(0, -h_2)/p_{iu}(h_1, 0)|$ of L-joints of lined ducts according to Figure 1(b), for different states of the corner wall: ——, absorbing; ----, rigid; ·–·–, soft. $h_1 = h_2 = 0{\cdot}2$ m, $d_1 = d_2 = 0{\cdot}1$ m, $\Xi_1 = \Xi_2 = 10$ kPa s/m^2.

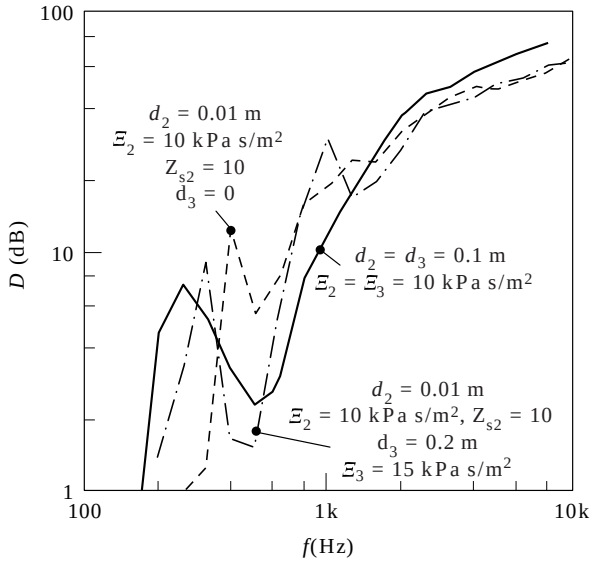

Figure 19. Frequency curves of the loss $D = 20 \lg |p_i(0, -h_2)/p_m(h_1, 0)|$ of L-joints of lined ducts according to Figure 1(b), for different states of the corner wall and of the exit duct. Other parameters as Figure 18.

$$-\sum_m D_n \gamma 2_n q 2_n(y)$$

$$\stackrel{!}{=} \sum_\alpha B_\alpha q' 3_\alpha(h_1)(e^{-\gamma 3_\alpha(y+h_2)} + R_\alpha\, e^{+\gamma 3_\alpha(y+h_2)}) + \sum_\beta C_\beta \gamma 4_\beta q 4_\beta(y)(1 - R_\beta). \quad (60b)$$

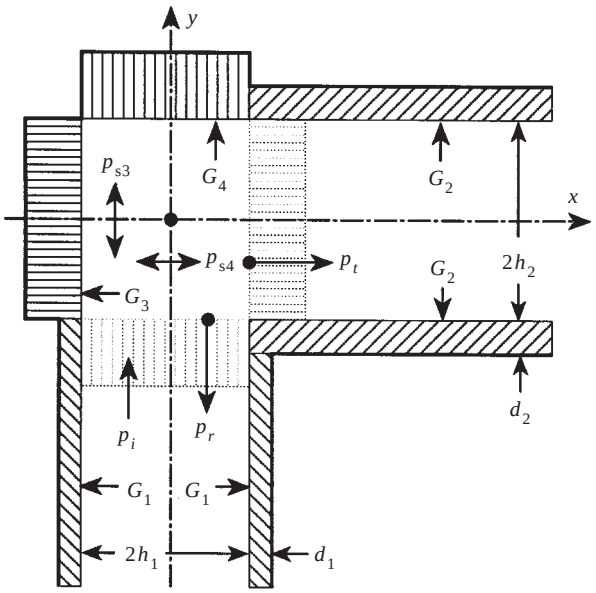

Figure 20. Lined ducts with a L-joint and absorbers at both corner walls; fictitious duct segments $i = 3, 4$; field components of a modal analysis.

The prime again indicates the derivative with respect to the indicated argument, here at the indicated place. These are four equations for four sets of amplitudes. The A_m will be eliminated from equations (59a, b) and the D_n from equations (60a, b). This is possible by the application of the orthogonality integrals with $q1_m(x)$ and $q2_n(y)$, respectively, by which procedure the integrals will appear:

$$S_{\alpha,k} := \frac{1}{2h_1}\int_{-h_1}^{h_1} q3_\alpha(x) q1_k(x)\,\mathrm{d}x = 0, \qquad \alpha + k = \text{odd}$$

$$= \frac{1}{2}\left[\frac{\sin(\varepsilon 3_\alpha - \varepsilon 1_k)h_1}{(\varepsilon 3_\alpha - \varepsilon 1_k)h_1} + (-1)^{(\alpha+k)/2}\frac{\sin(\varepsilon 3_\alpha + \varepsilon 1_k)h_1}{(\varepsilon 3_\alpha + \varepsilon 1_k)h_1}\right], \quad \alpha + k = \text{even}, \tag{61a}$$

$$T_{\beta,k} := \frac{1}{2h_2}\int_{-h_2}^{h_2} q4_\beta(y) q2_k(y)\,\mathrm{d}y = 0, \qquad \beta + k = \text{odd}$$

$$= \frac{1}{2}\left[\frac{\sin(\varepsilon 4_\beta - \varepsilon 2_k)h_2}{(\varepsilon 4_\beta - \varepsilon 2_k)h_2} + (-1)^{(\beta+k)/2}\frac{\sin(\varepsilon 4_\beta + \varepsilon 2_k)h_2}{(\varepsilon 4_\beta + \varepsilon 2_k)h_2}\right], \quad \beta + k = \text{even}. \tag{61b}$$

The zero value of the integrals for $\alpha + k = \text{odd}$ and $\beta + k = \text{even}$, respectively, follows from symmetry considerations. The special values $S_{\alpha,k} \to \delta_{\alpha,k} N1_k$ and $T_{\beta,k} \to \delta_{\beta,k} N2_k$ with the norms Ni_k of the modes in the ducts are important in numerical computations, when the (fictitious) duct section $i = 3$ has the same lining as the duct $i = 1$ and when the linings for $i = 4$ and $i = 2$ agree with each other. Further integrals are

$$Ia_{\beta,k} := \frac{1}{2h_1}\int_{-h_1}^{h_1} \mathrm{e}^{+\gamma 4_\beta x}\, q1_k(x)\,\mathrm{d}x, \qquad Ib_{\beta,k} := \frac{1}{2h_1}\int_{-h_1}^{h_1} \mathrm{e}^{-\gamma 4_\beta x}\, q1_k(x)\,\mathrm{d}x, \tag{62a}$$

$$IA_{\alpha,k} := \frac{1}{2h_2}\int_{-h_2}^{h_2} \mathrm{e}^{+\gamma 3_\alpha y}\, q2_k(y)\,\mathrm{d}y, \qquad IB_{\alpha,k} := \frac{1}{2h_2}\int_{-h_2}^{h_2} \mathrm{e}^{-\gamma 3_\alpha y}\, q2_k(y)\,\mathrm{d}y. \tag{62b}$$

The values of these are given in the previous sections (under different symbols). By application of

$$\frac{1}{2h_1}\int_{-h_1}^{h_1} \cdots q1_k(x)\,\mathrm{d}x \tag{63a}$$

to both sides of equations (59a, b) one gets

$$\delta_{\mu,k} P_i N1_\mu + A_k N1_k = \sum_\alpha B_\alpha (1 + R_\alpha) S_{\alpha,k} + \sum_\beta C_\beta q4_\beta(-h_2)(\mathrm{e}^{-\gamma 4_\beta h_1} Ia_{\beta,k}$$

$$+ R_\beta\, \mathrm{e}^{+\gamma 4_\beta h_1} Ib_{\beta,k}), \tag{64a}$$

$$\delta_{\mu,k} P_i \gamma 1_\mu h_2 N1_\mu - A_k \gamma 1_k h_2 N1_k = \sum_\alpha B_\alpha \gamma 3_\alpha h_2 (1 - R_\alpha) S_{\alpha,k}$$

$$- \mathrm{j} U_4 \sum_\beta C_\beta (-1)^\beta q4_\beta(h_2)(\mathrm{e}^{-\gamma 4_\beta h_1} Ia_{\beta,k} + R_\beta \, \mathrm{e}^{+\gamma 4_\beta h_1} Ib_{\beta,k}), \tag{64b}$$

and by the application of

$$\frac{1}{2h_2} \int_{-h_2}^{h_2} \cdots q2_k(y) \, \mathrm{d}y \tag{63b}$$

to both sides of equations (60a, b), one obtains

$$D_k N2_k = \sum_\alpha B_\alpha q3_\alpha(h_1)(\mathrm{e}^{-\gamma 3_\alpha h_2} IB_{\alpha,k} + R_\alpha \, \mathrm{e}^{+\gamma 3_\alpha h_2} IA_{\alpha,k}) + \sum_\beta C_\beta (1 + R_\beta) T_{\beta,k}, \tag{65a}$$

$$D_k \gamma 2_k h_1 N2_k = \mathrm{j} U_3 \sum_\alpha B_\alpha q3_\alpha(h_1)(\mathrm{e}^{-\gamma 3_\alpha h_2} IB_{\alpha,k} + R_\alpha \, \mathrm{e}^{+\gamma 3_\alpha h_2} IA_{\alpha,k})$$

$$- \sum_\beta C_\beta \gamma 4_\beta h_1 (1 - R_\beta) T_{\beta,k}. \tag{65b}$$

The A_k, D_k can be eliminated by multiplication of the first equation in pairs by $\gamma 1_k h_2$ or $\gamma 2_k h_1$ and addition or subtraction of the second equation, respectively. The result is

$$\sum_\alpha B_\alpha S_{\alpha,k} [\gamma 3_\alpha h_2 (1 - R_\alpha) + \gamma 1_k h_2 (1 + R_\alpha)]$$

$$+ \sum_\beta C_\beta (-1)^\beta q4_\beta(h_2)(\gamma 1_k h_2 - \mathrm{j} U_4)(\mathrm{e}^{-\gamma 4_\beta h_1} Ia_{\beta,k} + R_\beta \, \mathrm{e}^{+\gamma 4_\beta h_1} Ib_{\beta,k})$$

$$= 2\delta_{\mu,k} P_i \gamma 1_\mu h_2 N1_\mu, \tag{66a}$$

$$\sum_\alpha B_\alpha q3_\alpha(h_1)(\gamma 2_k h_1 - \mathrm{j} U_3)(\mathrm{e}^{-\gamma 3_\alpha h_2} IB_{\alpha,k} + R_\alpha \, \mathrm{e}^{+\gamma 3_\alpha h_2} IA_{\alpha,k})$$

$$+ \sum_\beta C_\beta T_{\beta,k} [\gamma 4_\beta h_1 (1 - R_\beta) + \gamma 2_k h_1 (1 + R_\beta)] = 0. \tag{66b}$$

The combination of equations (66a, b) is a linear, inhomogeneous system of equations ($k = 0, 1, 2, \ldots$) for the combined vector $\{\{B_\alpha\}, \{C_\beta\}\}$ of the mode amplitudes in the corner area. After its solution the amplitudes A_m can be computed from equation (64a) and the D_n from equation (65a). Then all fields are known and the task is solved. In numerical computations all mode orders m, n, α, β, k may run up to the same limit m_{hi}.

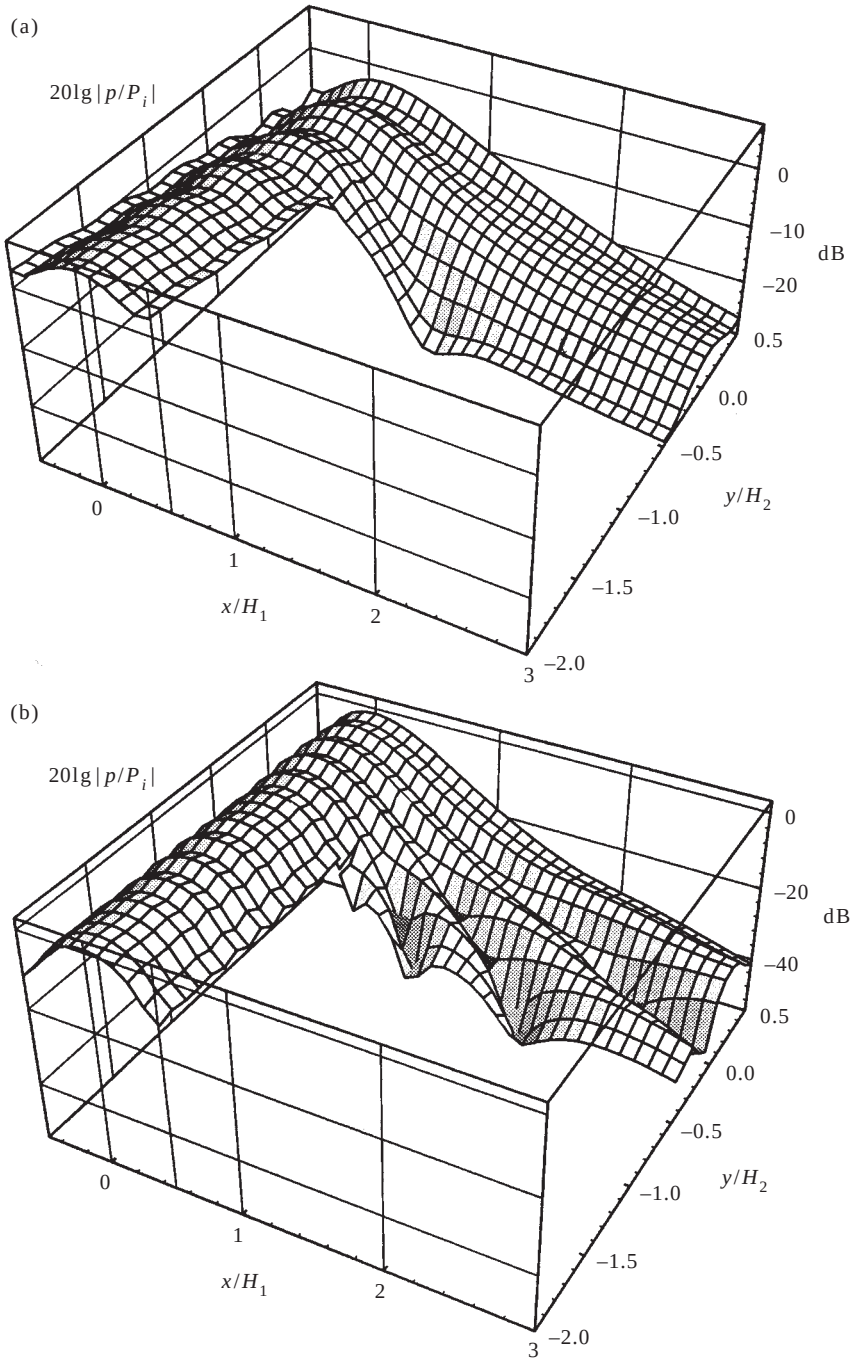

Figure 21. (a) 3D-plot of the sound pressure level in L-joints of lined ducts according to Figure 20, at $f = 1000$ Hz; the lining is identical everywhere; to be compared to Figures 11(a) and 12(a). $\mu = 0$, $m_{hi} = 8$, $h_1 = h_2 = 0{\cdot}2$ m, $d_1 = d_2 = d_3 = d_4 = 0{\cdot}1$ m, $\Xi_1 = \Xi_2 = \Xi_3 = \Xi_4 = 10$ kPa s/m^2. (b) As (a), but at $f = 2000$ Hz; the lining is identical everywhere; to be compared to Figures 11(b) and 12(b).

A "one-sided" modal analysis has been applied on the boundary conditions in the sense that the operations (63a, b) have been applied on both the pressure and the velocity conditions. Because the modes in the sections $i = 3, 4$ are orthogonal also, one can apply a "two-sided" modal analysis in which the operations (63a, b) are applied to the pressure condition, for example, and similar operations, after $q1_k(x) \rightarrow q3_k(x)$ in equation (63a) and $q2_k(y) \rightarrow q4_k(y)$ in equation (63b), are applied to the velocity conditions. The amplitudes A_m, D_n can also be eliminated after these operations. Experience shows that the precision of the two-sided modal analysis in the fitting of the fields is better than with a one-sided analysis; however the price for the higher precision is more complicated matrix terms in the system of equations (66) and longer computing times. The two-sided analysis, therefore, is not demonstrated here.

The amount of computation increases with the analysis of this section compared to the equations of the former sections for several reasons. First, in the most general case, four sets of modal solutions must be computed instead of two sets. Second, the upper limit m_{hi} of the mode orders must be higher; it increases with the frequency and duct width. A value of $m_{hi} = 8$ will be applied below, which is sufficient for the applied parameters. Third, even for the same limit m_{hi}, the size of the system of equations is two times the size of the earlier systems. On the other hand, a number of simplifications are possible, when the linings of the ducts and/or sections become identical. So, on average, the computing time with the present

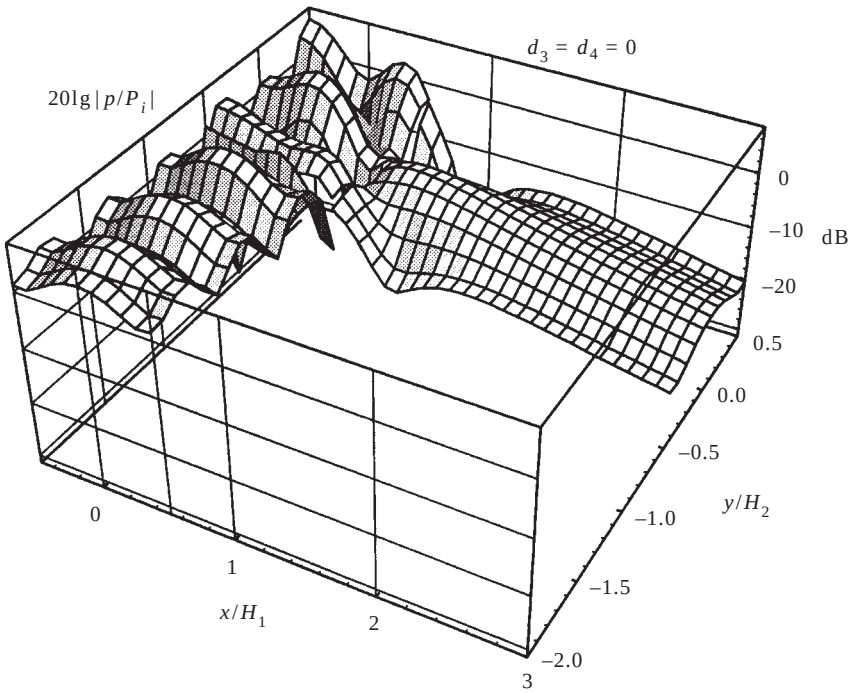

Figure 22. 3D-plot of the sound pressure level in L-joints of lined ducts according to Figure 20, at $f = 1000$ Hz; the corner walls are rigid. $\mu = 0$, $m_{hi} = 8$, $h_1 = h_2 = 0{\cdot}2$ m, $d_1 = d_2 = 0{\cdot}1$ m, $\Xi_1 = \Xi_2 = 10$ kPa s/m^2.

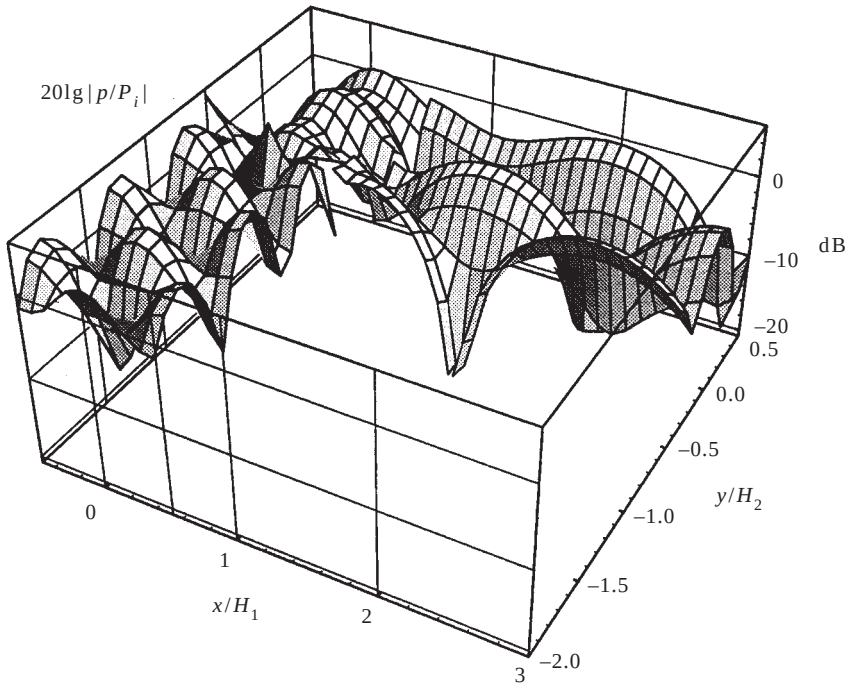

Figure 23. 3D-plot of the sound pressure level in L-joints of lined ducts according to Figure 20, at $f = 1000$ Hz; the corner walls are absorbing. $\mu = 0$, $m_{hi} = 8$, $h_1 = h_2 = 0{\cdot}2$ m, $d_1 = d_2 = 0$, $d_3 = d_4 = 0{\cdot}1$ m, $\Xi_3 = \Xi_4 = 10$ kPa s/m^2.

analysis is about twice the computing time with the analysis of section 3 and four times the computing time with the analysis of section 2.

Figures 21(a, b) are counterparts of Figures 11 and 12. If one compares values of sound pressure levels, it should be taken into account that the amplitude P_i of the incident wave, to which the levels are referred, is now defined in the orifice of duct 1, instead of the centre of the corner area as in the former sections. Therefore, the level contours are now shifted by about $-2{\cdot}2$ dB at $f = 1000$ Hz and by about $-0{\cdot}45$ dB at $f = 2000$ Hz. Now the waviness of the standing wave in the entrance duct is continued into the corner area more steadily, and also the profile in the x-direction agrees better with the profile of the incident wave. Both features of the result are plausible. The precision of the field matching in the end planes is sufficient.

The other 3D-plots of sound pressure levels are concerned with special cases. The ducts for Figure 22 are both absorbing, but the corner area is rigid on both sides. The standing wave pattern of the corner area produces a near field in the exit duct with predominant but quickly decaying higher modes. The transmission loss of the corner is evidently quite comparable in its value to those in the case of an absorbing corner area. This is in full contradiction to the initial guess in the introduction. The opposite situation is illustrated in Figure 23. Now the ducts are rigid and the corner walls absorbing. In fact, the average level in the corner area is somewhat reduced, but is still sufficiently high to produce strong, propagating higher modes in the exit duct, so that the transmission loss is evidently much

smaller than with an absorbing exit duct. Figure 24 illustrates a modification in which only the corner wall opposite to the entrance duct is lined with an absorber (now for $f = 2000$ Hz). Figure 25(a) illustrates well the mechanism for a high transmission loss of the corner (at $f = 500$ Hz). Now only the exit duct is lined; the other duct and corner walls are rigid. The field pattern in the y-direction in the corner area nearly corresponds to a pure anti-symmetrical mode of order $n = 1$ in the exit duct. It is strongly attenuated at 500 Hz. So the profile of the least attenuated mode in the exit duct appears at a rather low level after a relatively short near field range. This diagram again clarifies that a high transmission loss of a duct corner is primarily not a matter of absorption at the corner walls, but a matter of pattern matching at the entrance of the exit duct. Figure 25(b) repeats the arrangement of Figure 25(a), but now for a frequency of $f = 2000$ Hz. The pattern of the corner area is disturbed in the sense that it can no longer be represented by the pattern of one or a few higher modes of the exit duct, and the content of the pattern of the fundamental mode of the exit duct is higher. Therefore, the least attenuated mode "peels off" from the near field at a higher level than before.

The last diagram, Figure 26, collects frequency curves of the transmission loss of a number of conditions of absorption in the ducts and of the corner area. It shows the role of an absorber at the corner wall opposite the entrance duct: useful values of the transmission loss begin at lower frequencies with absorption than

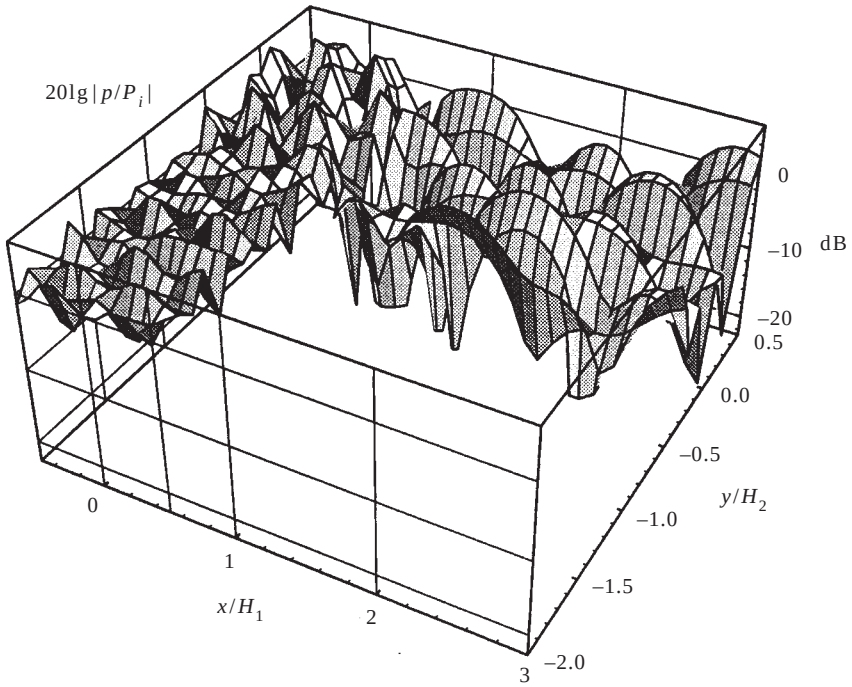

Figure 24. 3D-plot of the sound pressure level in L-joints of lined ducts according to Figure 20, at $f = 2000$ Hz; only the corner wall opposite the entrance duct is absorbing. $\mu = 0$, $m_{hi} = 8$, $h_1 = h_2 = 0{\cdot}2$ m, $d_1 = d_2 = d_3 = 0$, $d_4 = 0{\cdot}1$ m, $\Xi_4 = 10$ kPa s/m^2.

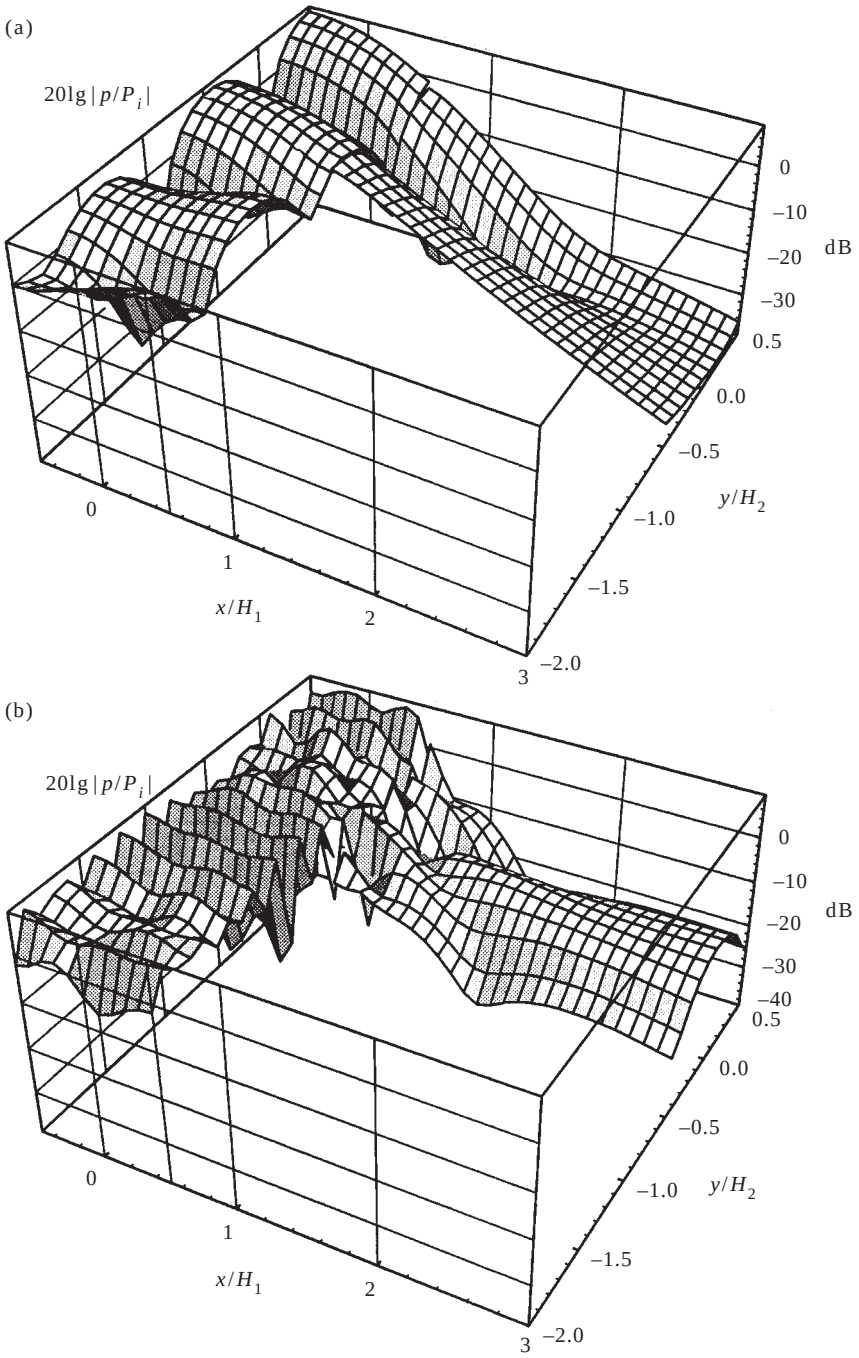

Figure 25. (a) 3D-plot of the sound pressure level in L-joints of lined ducts according to Figure 20, at $f = 500$ Hz; only the exit duct is absorbing. The standing wave pattern in the corner area corresponds well to the first higher mode pattern in the exit duct, which is cut off at this frequency. (b) As (a) but at $f = 2000$ Hz, only the exit duct is absorbing. The field pattern in the corner area has a higher content of the fundamental mode; the corner loss is smaller. $\mu = 0$, $m_{hi} = 8$, $h_1 = h_2 = 0{\cdot}2$ m, $d_1 = d_3 = d_4 = 0$, $d_2 = 0{\cdot}1$ m, $\Xi_2 = 10$ kPa s/m^2.

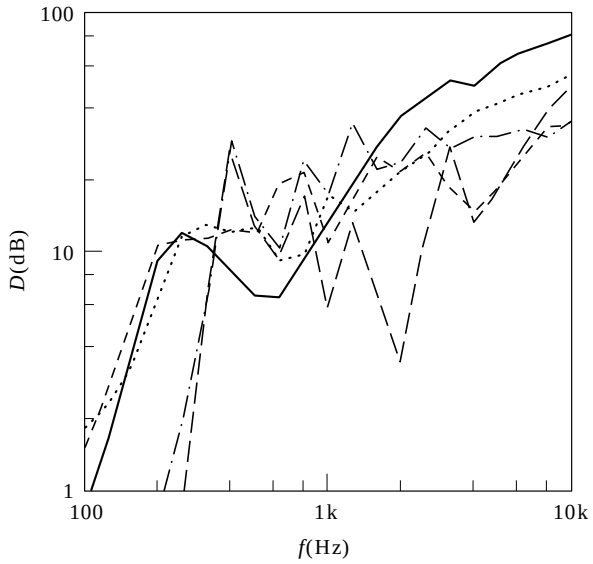

Figure 26. Loss $D = 20 \lg |p_i(0, -h_2)/p_u(h_1, 0)|$ of an L-joint according to Figure 20, with different states of the corner and of the ducts. $h_1 = h_2 = 0{\cdot}2$ m. ——, $d_1 = d_2 = d_3 = d_4 = 0{\cdot}1$ m, $\Xi_1 = \Xi_2 = \Xi_3 = \Xi_4 = 10$ kPa s/m^2; ----------, $d_1 = d_3 = 0$, $d_2 = d_4 = 0{\cdot}1$ m, $\Xi_2 = \Xi_4 = 10$ kPa s/m^2; ----, $d_1 = d_2 = 0$, $d_3 = d_4 = 0{\cdot}1$ m, $\Xi_3 = \Xi_4 = 10$ kPa s/m^2; — —, $d_1 = d_2 = 0{\cdot}1$ m, $\Xi_1 = \Xi_2 = 10$ kPa s/m^2, $d_3 = d_4 = 0$; ——-—-, $d_1 = d_2 = d_3 = d_4 = 0$.

without absorption in that place. Rigid walls of the corner area can produce high attenuation peaks at some frequencies, but they also generate dips of the transmission loss at other frequencies. Smooth frequency curves of the transmission loss need absorbing corner walls and a sufficient attenuation in the exit duct.

The question is, over what length the exit duct should be lined. The general answer is: until the end of the near field of the higher modes. The diagrams show that a lined segment with a length of about 2 to 3 times the duct width H_2 will be sufficient in many cases; the design of a length of about $5H_2$ will be safe in most cases. Then even the least attenuated mode will produce a negligible feedback on the corner area when it is reflected after that distance.

5. DERIVED DUCT AND CORNER SHAPES

First, the restriction to two-dimensional ducts is realised. When the duct has the constant dimension b in the z-direction and constant boundary conditions at the walls normal to that direction (e.g., rigid), then the incident wave and all fields and field components will be augmented by a mode profile factor $q_\kappa(z)$ which can be dropped in the computations for the mode amplitudes. The only modification will be for γi_k in equation (3). There, an additional term $+\varepsilon_\kappa^2$ will appear if the mode profile has the shape $q_\kappa(z) = \cos(\varepsilon_\kappa z)$; $= \sin(\varepsilon_\kappa z)$. With rigid walls normal to the z-axis the modal wave numbers are $\varepsilon_\kappa b = \kappa\pi$ and $\varepsilon_\kappa b = (\kappa + 1/2)\pi$, $\kappa = 0, 1, 2, \ldots$, for symmetrical and anti-symmetrical waves, respectively. If the

walls are lined, $\varepsilon_\kappa b$ must be computed from the corresponding characteristic equation.

The computing schemes of the previous sections are applicable not only to L-joints of ducts. When the modal reflection factors in sections 2 and 4 at G_3 are set to $r_n = 0$, then they describe an infinitely long branch of a T-joint in which the incident wave comes from the side branch. If the reflection factors at G_3 in section 3 and at G_4 in section 4 are set to $r_n = 0$, then one has the analysis for a T-joint in which now the incident wave comes from the through-going branch. If in section 4 the reflection factors both at G_3 and at G_4 are assumed to be zero, then a cross-joint of ducts is described.

As was stated already, the analysis of section 4 is immediately applicable to rigid ducts. The equations of the earlier sections 2 and 3 can be applied to joints of ducts having rigid *outer* duct (and corner) walls. For that, the rigid walls are placed into the co-ordinate planes, the inner halves of the ducts and of the corner are taken and the duct modes are restricted to symmetrical shapes (i.e., in our convention to even orders). It is, however, not possible in general to handle the outer halves of the ducts and of the corner (with rigid co-ordinate planes) by the theories of sections 2 and 3. This means that rigid walls at the *inner* sides of the ducts and corner cannot be treated by the theories of those sections. The reason is that then the auxiliary source V_q lies in the extension of a rigid plane. The duct modes, in which V_q shall be developed, all have zero velocity in that plane; so it is impossible to apply that development. The plane which contains V_q must be absorbing in order that the component duct modes for V_q have a finite velocity normal to that plane.

Finally, it is mentioned—without more detailed discussion—that the schemes of the previous theories can also be applied to ducts with bulk reacting linings. The main difference in the analysis will come from the more complicated shape of the orthogonality relation of modes in ducts with bulk reacting linings. How this orthogonality relation is applied to boundary conditions in ducts is shown in reference [12, Vol. III].

6. CONCLUDING REMARKS

The results presented above show that the original idea, according to which the absorption of sound rays at walls opposite the entrance duct would produce high transmission losses of a duct corner, must be revised. It is not so much the absorption at the corner walls which produces the transmission loss, but the higher mode excitation in the exit duct by pattern matching of the standing wave pattern in the corner area to the mode patterns in the exit duct. These higher modes must then be effectively attenuated, which—at high frequencies—requires an absorbing lining of a certain length of the exit duct. Examples are shown in which rigid corner walls are combined with high transmission loss values.

The application of the theories presented supposes the availability of a fast computing program for the generation of sets of modal solutions of the characteristic equation in lined ducts, which is robust with respect to "mode jumping". Such algorithms are described in references [12, Vol. III] and [13].

REFERENCES

1. L. Cremer 1953 *Acustica*, *Akustische Beihefte* **3**, 249–263. Theorie der Luftschall-Dämpfung im Rechteckkanal mit schluckender Wand und das sich dabei ergebende höchste Dämpfungsmaß.
2. C. P. Brittain, C. R. Maguire, R. A. Scott and A. J. King 1948 *Engineering* (*London*) **165**, 97–98, 145–147. Attenuation of sound in lined air ducts.
3. W. K. R. Lippert 1954 *Acustica* **4**, 313–319. The measurement of sound reflection and transmission at right angled bends in rectangular tubes.
4. W. K. R. Lippert 1955 *Acustica* **5**, 274–278. Wave transmission around bends of different angles in rectangular ducts.
5. M. Hubert and A. Said 1973 *DAGA Tagungsberichte*, 347. Reflexions- und Transmissionsfaktor eines 90°-Knickes in einem Kanal mit rechteckigem Querschnitt.
6. T. L. Redmore and K. A. Mulholland 1962 *Journal of Sound and Vibration* **8**, 373–375. The application of mode coupling theory to the transmission of sound in the sidebranch of a rectangular duct system.
7. J. C. Bruggeman 1987 *Journal of Acoustical Society of America* **82**, 1045–1051. The propagation of low frequency sound in a two-dimensional duct system with T-joints and right angle bends.
8. A. Cummings 1978 *Journal of Sound and Vibration* **61**, 347–373. The attenuation of lined plenum chambers in ducts, I: theoretical models.
9. A. D. Lapin 1961 *Soviet Physics Acoustics* **7**, 171–175. Sound propagation in a wave guide with side branches and volume resonators in the walls.
10. A. D. Lapin 1967 *Soviet Physics Acoustics* **12**, 286–290. Application of resonators for the enhancement of sound attenuation in a waveguide lined with a soundproofing material.
11. Young-Chung Cho 1980 *Journal of the Acoustical Society of America* **67**, 1421–1426. Reciprocity principle in duct acoustics.
12. F. P. Mechel *Schallabsorber* 1989, *Vol*. I *Äußere Schallfelder*, *Wechselwirkungen*; 1995, *Vol*. II *Innere Schallfelder*, *Strukturen*; 1998, *Vol*. III *Anwendungen*. Stuttgart: S. Hirzel Verlag.
13. F. P. Mechel 1991 *Acustica* **73**, 223–239. Modal solutions in rectangular ducts lined with locally reacting absorbers.